

2025

Quantifying mechanobiology using precision cut mouse lung slices

<https://hdl.handle.net/2144/52327>

"Downloaded from OpenBU. Boston University's institutional repository."

BOSTON UNIVERSITY

ARAM V. CHOBANIAN & EDWARD AVEDISIAN SCHOOL OF MEDICINE

Thesis

**QUANTIFYING MECHANOBIOLOGY USING PRECISION CUT MOUSE
LUNG SLICES**

by

ERIKA LIN

B.S., University of California, Irvine 2018
M.S., University of Chicago, 2019

Submitted in partial fulfillment of the
requirements for the degree of
Master of Science

2025

© 2025 by
ERIKA LIN
All rights reserved

Approved by

First Reader

Aaron W. Young, Ph.D.
Assistant Professor of Pharmacology, Physiology, & Biophysics

Second Reader

Ramaswamy Krishnan, Ph.D.
Associate Professor of Emergency Medicine
Harvard Medical School

DEDICATION

I would like to dedicate this work to my family, partner, and friends. To the Lin family, Ama, Dad, Mom, Gugu, and Bry – I am so grateful for your endless sacrifices, so that I can dream big on our behalf. To my partner, Nar, thank you for believing in me (even more than myself). To my wonderful friends, I am a reflection of you all. I would not be where I am today without your ongoing support.

ACKNOWLEDGMENTS

After 4 years of translational research on chronic lung disease of infancy, I desired to learn even more about lung and the effects of mechanical ventilation that I frequently witnessed in the neonatal intensive care unit. At this point in my training, I had only worked with basic scientists, data scientists, and physicians. I had the fortunate opportunity to train with innovative engineer scientists in Dr. Ramaswamy Krishnan's lab at Beth Israel Deaconess Medical Center. One of the most valuable lessons I gained from the Krishnan Lab is that we all have the same goal, but the ways in which we approach that goal can differ and has significantly enriched my learning.

Rama, thank you for challenging me to take a step back and think critically and meticulously about my work. In the future, I hope to lead with the same positivity and proactive mentorship that you have shown me. Your passion for discovering new knowledge is refreshing! Jae, thank you for always patiently answering my many questions. I am grateful for the extensive time you have invested in training me on many valuable techniques that I will take with me into my future career. Your dedication to pushing the boundaries of basic science is inspiring. Niccole, thank you for helping me through techniques and experiments no matter how busy you may be. My experiments could not happen without your meticulous preparation and critical feedback. I admire your intelligence, resourcefulness, and collaborative spirit. You are a wonder woman! Jackie, thank you for paving the way for me. Your elaborate protocols and dedicated personal trainings allowed me to seamlessly transition into the lab.

QUANTIFYING MECHANOBIOLOGY USING PRECISION CUT MOUSE

LUNG SLICES

ERIKA LIN

ABSTRACT

Rationale: Acute respiratory distress syndrome (ARDS) is a multi-factorial respiratory syndrome that eventually leads to an acute inflammation disorder called acute lung injury (ALI). To investigate upstream stimuli and downstream mechanistic changes, precision cut lung slices (PCLS) have emerged as a valuable pre-clinical model. We focused on the ALI subgroup known as ventilator-induced lung injury (VILI). Using a custom culture platform, we worked to establish a PCLS-based model system of VILI. We hypothesized that this model system could cyclically stretch murine PCLS (mPCLS) over a 24-hour period, while preserving sterility and viability. We hypothesized further that the experiments can be achieved in a 12-well format.

Objectives: To optimize a developed and validated mechanotransduction bioassay system for high-throughput use. Additionally, by optimizing the *in vitro* system, adherence and metabolic signal scopes can be enhanced and preserved in the setting of cyclical stretch.

Methods: 1) mPCLS adherence was tested on two membrane compositions (NuSil® Gel-8100 vs. bare) prepared on a stretchable silicone membrane, and on variable air blowing times which reinforced adhesion. 2) mPCLS were plated on a custom 6-well “FlexFrame” plate, incubated for 24 hours in a sterile incubator on an established 12-well stretching device with programmed cyclical stretch parameters. 3) mPCLS were

quantified for sterility with visual inspection of spores and viability using the commercially available MTT assay.

Results: mPCLS successfully remained adhered to the NuSil®-coated membrane with air blowing of 20 seconds (20 psi). NuSil® adhesive did not release toxic byproducts that decrease viability. Adhered mPCLS were cyclically stretched for 24 hours at 37°C to model *in vivo* mechanical ventilation and maintained viability. Cyclical stretching did not affect mPCLS sterility and viability.

Conclusions: By generating novel insights on PCLS adherence and viability with a new adhesive, air blowing conditions, and establishing metabolic signal scopes, we optimized an *in vitro* high-throughput mechanotransduction bioassay system. This foundational work enhances our ability to study VILI-related symptoms and pursue future studies on cellular mechanics, inflammatory cytokines, and airway contractility in murine and human PCLS with different genetic profiles and disease conditions.

TABLE OF CONTENTS

DEDICATION	iv
ACKNOWLEDGMENTS	v
ABSTRACT	vi
TABLE OF CONTENTS	viii
LIST OF TABLES	x
LIST OF FIGURES	xi
LIST OF ABBREVIATIONS	xiii
INTRODUCTION	1
Lung Anatomy and Physiology	1
Pathophysiology of Acute Respiratory Distress Syndrome.....	3
Current Treatment for ARDS	4
Ventilator-Induced Lung Injury	6
Mechanics of Ventilator Induced Lung Injury	8
Precision Cut Lung Slices.....	11
HYPOTHESIS	14
AIMS.....	14
METHODS	15
Precision Cut Lung Slices.....	15
Elastic Membrane Preparation.....	17
NuSil® Adhesive	19
mPCLS Treatment	20

Adhering and Plating mPCLS.....	20
Multi-Well Stretcher	22
Setting Up Experimental Plate Conditions	24
Measuring Cell Viability.....	26
Statistics	26
RESULTS	27
Verifying Stretch Calibration.....	27
Establishing mPCLS Adherence Conditions	28
Enhancing mPCLS Metabolic Signal Scope.....	29
Quantifying Viability After Adherence	33
Visualizing and Quantifying Adhesion.....	34
Quantifying Viability	36
DISCUSSION.....	39
CONCLUSION.....	46
BIBLIOGRAPHY	48
CURRICULUM VITAE.....	53

LIST OF TABLES

Table 1. Berlin definition highlighting 4 categories of multi-factorial ARDS	4
Table 2. Categories of VILI based on injury mechanism and associated adverse outcomes	8
Table 3. Static ventilator variables and mechanisms of action	9
Table 4. Dynamic ventilator variables and mechanisms of action	10

LIST OF FIGURES

Figure 1. Schematic of the role of PCLS to study multi-factorial mechanisms of lung remodeling	13
Figure 2. Schematic of MTT biochemical mechanism of action.....	13
Figure 3. Schematic of PCLS workflow from harvest to application.....	16
Figure 4. Schematic of different experiments involving a PCLS lung airway	17
Figure 5. Customized elastic membrane and FlexFrame assembly	18
Figure 6. NuSil® adhesive preparation	19
Figure 7. Experimental mPCLS were air blown at 20 psi for 20 seconds	21
Figure 8. FlexFrame with adhered mPCLS on sticky elastic membrane (n=6) for cyclical stretching.....	21
Figure 9. Mechanotransduction bioassay system components	23
Figure 10. <i>In vitro</i> application of cyclical stretching on mPCLS	23
Figure 11. Experimental conditions to evaluate adherence and viability	25
Figure 12. The working mechanotransduction bioassay system was calibrated prior to beginning stretch experiments	27
Figure 13. Flowchart detailing the workflow of optimizing PCLS adherence	28
Figure 14. MTT assay was successfully validated on actively cultured human airway smooth muscle (hASM) cells.....	30
Figure 15. HCl is not necessary to optimize viability measurement in MTT-treated mPCLS.....	31

Figure 16. The absorbance of MTT-treated mPCLS measured with and without supernatant were not significantly different	32
Figure 17. MTT-treated mPCLS demonstrated measurable signal scope validating adaption of MTT assay to tissue	32
Figure 18. mPCLS adherence with NuSil® and air blow does not compromise viability.	34
Figure 19. Adhered mPCLS were stretched at customized parameters.....	35
Figure 20. Adhered mPCLS demonstrated a direct relationship with stretch and percent change in area strain.....	36
Figure 21. 4/6 mPCLS were adhered or partially adhered after 24 hours of cyclical stretching.....	37
Figure 22. Cyclical stretching of mPCLS does not affect viability	38
Figure 23. Schematic of atelectrauma, volutrauma, barotrauma, and biotrauma on the macroscopic lung and alveolar microenvironment.....	40

LIST OF ABBREVIATIONS

Acute lung injury.....	ALS
Acute respiratory distress syndrome.....	ARDS
Analysis of Variance.....	ANOVA
Carbon dioxide.....	CO ₂
DMEM/F-12.....	Dulbecco's Mod. Of Eagle's Medium/Ham's F-12 50/50 Mix with L-glutamine and 15 mM HEPES
Hank's Balanced Salt Solution.....	HBSS
Hertz.....	Hz
Human precision cut lung slices.....	hPCLS
Human airway smooth muscle.....	hASM
Hydrochloric acid.....	HCl
Intensive care unit.....	ICU
Murine precision cut lung slices.....	mPCLS
((3-(4,5-dimethylthiazol-2-yl)-2,5-diphenyltetrazolium bromide).....	MTT
Nasal intermittent positive pressure ventilation.....	NIPPV
Plateau airway pressure.....	Pplat
Positive end-expiratory pressure.....	PEEP
Precision cut lung slices.....	PCLS
Ratio of arterial oxygen pressure to fractional inspired oxygen.....	PaO ₂ /FiO ₂
Ventilator induced lung injury.....	VILI

INTRODUCTION

Lung Anatomy and Physiology

The lungs are the primary organs of the respiratory system. The lungs are under constant cyclical stretch, facilitating exchange of gases, such as oxygen and carbon dioxide, between the environmental air and the blood, allowing our bodies to maintain ideal oxygen, carbon dioxide, and pH balance.^{8, 21}

The lungs can be organized into two functional zones, the conducting and respiratory zones. The conducting zone structures are not directly involved with gas exchange but create physical passageways for air to move in and out of our bodies. The primary entrance and exit of the respiratory system is the nose where atmospheric air enters the nares and into the nasal cavity separated by the nasal septum. The pseudostratified ciliated columnar epithelium has several functions including mucus production to trap foreign debris, move mucus and debris from nasal cavity, and shuttle materials towards the throat. The extensive capillary network and moist epithelium warms and humidifies the inhaled air. The pharynx is continuous with nasal cavities and is connected to the trachea by the larynx, a cartilaginous structure that regulates the volume of air that enters and leaves the lungs. The trachea extends from the larynx to the lungs and branches at the carina into left and right sided bronchi. The bronchi branch and allow air passage in and out of the lung. From the final bronchi, terminal bronchioles branch off leading into the respiratory zone.⁸

The respiratory zone structures are directly involved with gas exchange. The respiratory zone begins when the terminal bronchioles join the respiratory bronchioles

extending into the alveolar ducts ending at attached clusters of small grape-like sacs compromised of elastic fibers, which are termed alveoli. The expansion and recoiling of the alveoli control the surface area for gas diffusion and metabolic exchange. The simple squamous epithelium of the alveolar septum, type I alveolar cells, type II alveolar cells, alveolar macrophages, and endothelial cells comprise an alveolar epithelial-endothelial barrier.^{8,21} Type I alveolar cells comprise most of the surface area, while type II alveolar cells produce surfactant. Surfactant, a phospholipid and protein-rich substance, reduces alveolar surface tension to optimize gas exchange. Finally, alveolar macrophages are immune cells that phagocytize unwanted debris and pathogens surrounding the alveoli. In this selective air-blood barrier, the respiratory membrane allows simple diffusion of oxygen from alveoli to systemic blood in exchange for carbon dioxide to be released back into the atmosphere.^{8,20}

Human lung diseases can be classified as obstructive or restrictive. Obstructive lung diseases impair exhalation, such as asthma and chronic obstructive pulmonary disorder. Restrictive lung diseases impair lung expansion thereby decreasing lung volume, such as pneumoconiosis and acute respiratory distress syndrome (ARDS).⁸ When the alveolar epithelial-endothelial barrier is compromised, fluid and proteins have increased permeability and leak into the alveoli. The leaked proteins can interfere with surfactant production, metabolism, and function decreasing alveolar surface tension and increasing the risk for airway collapse and abnormal gas exchange.²⁹

Pathophysiology of Acute Respiratory Distress Syndrome

ARDS is a multi-factorial and complex syndrome with variable global and national estimates, especially with the 2019 coronavirus pandemic increasing these numbers. On a global scale, there is 10% incidence, with increased incidence in intensive care unit (ICU) settings. There are approximately 5.5 cases per ICU bed.¹¹ In the United States, there are approximately 200,000 cases per year, thus classifying it as a rare disease.³ ARDS involves direct pulmonary and extra pulmonary damage to alveoli resulting in an oxygenation disorder.⁶ Due to multifactorial injuries, such as pneumonia, drowning, or lung transplants, ARDS is characterized by an inflammatory response to damaged epithelial barriers and is further exacerbated by mechanical ventilation.⁶ Histologically, there is diffuse inflammation of the alveolar epithelium. Clinically, there is evidence of hypoxia, opaque chest imaging, and decreased lung compliance.

There are 3 phases of ARDS describing repair of the alveolar epithelium, reabsorption of edema, and fibrosis: exudative, proliferative, and fibrotic. In the exudative phase, the alveolar epithelium and endothelium is damaged resulting in exudate accumulation, immune cell infiltration, and subsequent proinflammatory cytokines release, such as IL-6.^{5, 10} The inflammatory environment impairs vascular flow and surfactant production by type II alveolar cells. In the proliferative phase, response to the acute exudative phase occurs, such as thickening of the alveolar septum, accumulation of alveolar cells, and early fibrosis.⁵ In the fibrotic phase, fibroblasts proliferate and deposit collagen in response to the damage to the alveolar epithelium and endothelium. Physiologically, the fibrotic phase results in decreased lung compliance and hypoxia.²⁴

While these downstream sequelae are now widely appreciated and intensively studied, upstream initiating mechanisms of ARDS are poorly understood. To this end, cellular, tissue, and animal models of ARDS are invaluable. A systemic cause-effect relationship of ARDS inducing stimuli requires dedicated investigation. By leveraging the unique advantage of a PCLS-based high-throughput platform, we have proposed to study the cause-effect relationships in ARDS.

Current Treatment for ARDS

In June 2012, a task force was formed to develop a clinical grading criteria for ARDS. The Berlin definition was established to categorize ARDS as mild, moderate, or severe based on specific oxygenation thresholds as an indication of lung function. The four major grading categories included timing, chest imaging outcomes, edema origins, and the ratio of the arterial partial pressure of oxygen to the fraction of inspired oxygen ($\text{PaO}_2/\text{FiO}_2$) (Table 1)

Table 1. Berlin definition highlighting 4 categories of multi-factorial ARDS.³³

Acute Respiratory Distress Syndrome	
Timing	Within 1 week of a known clinical insult or new or worsening respiratory symptoms
Chest imaging ^a	Bilateral opacities—not fully explained by effusions, lobar/lung collapse, or nodules
Origin of edema	Respiratory failure not fully explained by cardiac failure or fluid overload Need objective assessment (eg, echocardiography) to exclude hydrostatic edema if no risk factor present
Oxygenation ^b	
Mild	$200 \text{ mm Hg} < \text{PaO}_2/\text{FiO}_2 \leq 300 \text{ mm Hg}$ with PEEP or CPAP $\geq 5 \text{ cm H}_2\text{O}^c$
Moderate	$100 \text{ mm Hg} < \text{PaO}_2/\text{FiO}_2 \leq 200 \text{ mm Hg}$ with PEEP $\geq 5 \text{ cm H}_2\text{O}$
Severe	$\text{PaO}_2/\text{FiO}_2 \leq 100 \text{ mm Hg}$ with PEEP $\geq 5 \text{ cm H}_2\text{O}$

Abbreviations: CPAP, continuous positive airway pressure; FiO_2 , fraction of inspired oxygen; PaO_2 , partial pressure of arterial oxygen; PEEP, positive end-expiratory pressure.

^aChest radiograph or computed tomography scan.

^bIf altitude is higher than 1000 m, the correction factor should be calculated as follows: $[\text{PaO}_2/\text{FiO}_2 \times (\text{barometric pressure}/760)]$.

^cThis may be delivered noninvasively in the mild acute respiratory distress syndrome group.

Currently, there are relatively few effective ARDS treatments, which are categorized into pharmacological, mechanical ventilation, and supplemental management. In pharmacological management, several interventions have been trialed including beta-2 agonists to increase sodium transport on type I and type II alveolar cells to reduce pulmonary edema, keratinocyte growth factor to repair and restore damaged alveolar epithelium, and statins to mitigate overall inflammation.

In mechanical ventilation management, the primary goal is to reduce the workload of the respiratory muscles and optimize gas exchange. Mechanical ventilation management utilizes a reduced tidal volume approach, which is believed to reduce the likelihood of volutrauma. Additionally, reducing cyclic tidal recruitment, or repeated opening and closing of alveoli per breath, can reduce atelectrauma. High frequency oscillatory ventilation (HFOV) utilizes small tidal volumes and high mean airway pressures to lower volutrauma and atelectrauma. Lung recruitment maneuvers can also be included and involve applying a brief period of high airway pressure to reinflate collapsed alveoli, allowing for increased alveolar ventilation and gas exchange. Nasal intermittent positive pressure ventilation (NIPPV), considered a non-invasive ventilation, utilizes intermittent higher positive pressures to deliver oxygen via a mask over the nose and/or mouth.

Finally, supplemental management includes extracorporeal carbon dioxide (CO₂) removal from the blood to compensate for the compromised lung's inability to exchange appropriate amounts of CO₂. Prone positioning can also increase more uniform lung inflation and equal distribution of mechanical forces throughout the injured lung, leading

to better gas exchange and oxygenation of the blood. Of these management techniques, studies using prone positioning and NIPPV have shown beneficial outcomes.⁷

This sobering reality highlights the currently limited management of ARDS. To meet the therapeutic gap, a “one-size-fits all” solution may not be feasible due to the heterogeneous nature of ARDS. Several therapeutic candidates are being actively pursued, like the BIO-11006 peptide (BioMarck Pharmaceuticals), administered to ARDS patients on mechanical ventilation to inhibit the membrane-associated Myristoylated Alanine-Rich C-kinase protein. InflaRx’s Gohibic (vilobelimab), which targets the complement component of C5a, and received emergency use authorization by the Food and Drug Administration for COVID-19 patients on mechanical ventilation or extracorporeal membrane oxygenation in April 2023.²⁷ Overall, BIO-11006 and Gohibic substrates prevented an inflammatory cytokine storm. But it is unclear if these compounds have salutary effects towards restoring mechanotransduction. Lastly, cell-based therapies targeting natural killer T cells (agenT-797) reduced bacterial pneumonia and improved overall survival rates for patients on mechanical ventilation.¹

Screening, selection, and therapeutic prioritization requires effective drug discovery assays to recapitulate the cause-effect relationship in ARDS, such as inflammation, cell signaling mechanisms, and mechanotransduction. This thesis work aimed to optimize a high-throughput model system designed to fill in these gaps.

Ventilator-Induced Lung Injury

Patients experiencing an acute lung injury may benefit significantly from mechanical ventilation to alleviate the respiratory muscles’ efforts and optimize systemic

gas exchange.³¹ However, an unfortunate consequence of mechanical ventilation is ventilator-induced lung injury (VILI). VILI is characterized by excessive pressure, volume, and oxygen delivery causing repeated cycles of inflation or deflation beyond the lung's physiological expansion capacity.^{8,21} VILI can further introduce a secondary structural lung injury to the airways and parenchyma triggering a systemic inflammatory response that may increase a patient's risk for organ failure and death. Inflammatory characteristics include increased numbers of inflammatory cell infiltrates, such as alveolar macrophages and neutrophils, pro-inflammatory cytokine expression, hyaline membranes with proteins and dead cell debris lining alveoli, increased vascular permeability, and pulmonary edema.^{19,31}

Physiologically, VILI is primarily due to increased transpulmonary pressure, which is the pressure difference inside the alveoli and surrounding pleural space. The positive-pressure ventilation results in excessive positive end expiratory pressure (PEEP), which can damage the lungs.¹⁷

VILI can be categorized into various types based on injury mechanism: barotrauma, volutrauma, atelectrauma, oxygen toxicity, biotrauma, and shear stress (Table 2).

Table 2. Categories of VILI based on injury mechanism and associated adverse outcomes.³⁰

Type of VILI	Injury Mechanism	Adverse Outcomes
Barotrauma	Excessive pressure	<ul style="list-style-type: none"> • Over distension of alveoli • Risk for pneumothorax • Subcutaneous emphysema
Volutrauma	Excessively large tidal volumes	<ul style="list-style-type: none"> • Over distension of alveoli • Inflammation • Long-term injury to lung tissue
Atelectrauma	Repetitive opening and closing of collapsed alveoli	<ul style="list-style-type: none"> • Shearing forces on alveolar walls • Alveolar inflammation • Increased alveolar permeability
Oxygen toxicity	Chronic exposure to high oxygen concentrations	<ul style="list-style-type: none"> • Epithelial cell damage • Oxidative stress • Inflammation and cell death
Biotrauma	Systemic inflammation activating release of pro-inflammatory cytokines	<ul style="list-style-type: none"> • Worsen acute lung injury • ARDS pathogenesis
Shear stress	Significant difference in the pressure or volume between pulmonary structures (i.e. airways, alveoli)	<ul style="list-style-type: none"> • Mechanical disruption at the air-blood barrier

Mechanics of Ventilator Induced Lung Injury

VILI is characterized by regional lung over distention, reduced lung compliance, and increased tissue vulnerability to mechanical forces of ventilation.³² Ventilator variables are categorized as static and dynamic. Static variables include peak airway

pressure, plateau airway pressure (Pplat), PEEP, driving pressure, and tidal volume (Table 3).³⁰ Dynamic variables include respiratory rate, airflow amplitude, and inspiratory time fraction (Table 4).³⁰

Table 3. Static ventilator variables and mechanisms of action.^{30, 39}

Static Ventilator Variables	Description	VILI Mechanism
Peak airway pressure	Maximum inspiratory pressure dependent on elastic (airway), resistive (lung tissue), and equipment (i.e. endotracheal tube diameter and length) properties	<ul style="list-style-type: none"> • Too high • Impairs right ventricle filling • Pulmonary edema • Capillary stress • Endothelial cell injury • Ventricular failure and dilation
Plateau airway pressure (Pplat)	Stopping airflow at end of inspiration (<i>end-inspiratory alveolar pressure</i>)	<ul style="list-style-type: none"> • Too high • Over distension • Sensitive to tidal volume and respiratory compliance differences
Positive end expiratory pressure (PEEP)	Maintenance of positive expiratory pressure (<i>static preload</i>)	<ul style="list-style-type: none"> • Personalized to patient's lung physiology • Ensure small airways and alveoli do not collapse
Driving pressure*	(Driving pressure = Pplat – PEEP) Pressure required to open alveolar sacs	<ul style="list-style-type: none"> • Higher driving pressure = lower lung compliance (more “stiff”)
Tidal volume	Amount of air exchanged after normal breathing in and out of lung	<ul style="list-style-type: none"> • Higher tidal volumes = higher driving pressure

Table 4. Dynamic ventilator variables and mechanisms of action.^{30, 37}

Dynamic Ventilator Variables	Description	VILI Mechanism
Respiratory rate	Number of breaths per minute	<ul style="list-style-type: none"> • Maintain minute ventilation • Adjust to meet metabolic needs
Airflow amplitude	In a single breath, change in volume of air moving in and out of lungs	<ul style="list-style-type: none"> • Controls delivered volume and flow rate
Inspiratory time fraction*	Time spent inhaling to time spent inhaling + exhaling	<ul style="list-style-type: none"> • Controls duration of inhalation compared to entire breath cycle (inhalation + exhalation)

This thesis work leveraged a PCLS-based model system of VILI to more specifically investigate categories of VILI including volutrauma, biotrauma, and stretch. Some ventilator parameters that could be feasibly studied in our lab's established cyclical stretching device²² included Pplat, PEEP, tidal volume (static stretch), and respiratory rate (dynamic stretch). A major weakness of the system is that it does not recapitulate blood flow and associated shear stress. Additionally, all ventilator parameters could not physically be studied given certain anatomical components of the whole lung, such as the trachea, are not preserved in PCLS. Despite this, several airways that branch from the trachea, including alveoli, parenchyma, and multiple cell populations were captured in a PCLS. Thus, the living PCLS was an invaluable experimental tool to not only represent

native lung structure and microenvironment, but also study the effects of stretch magnitude, duration, and frequency in a living, multicellular system.¹⁶

Compared to traditional cellular models, PCLS included multicellularity and realistic cellular and ECM interactions. Thus, PCLS can be precisely stretched to specific magnitude and patterns and exclusively quantified to study specific outcomes, like stretching. Compared to animal models, PCLS are quickly obtained from specific donor types with direct inferential and biological measurements. Additionally, drug studies required large sample populations that PCLS are more readily available to fill. As a result, PCLS were a bridge between cellular and organ-based pre-clinical models to study intricate mechanisms of diseased and non-diseased lungs.¹⁵

Precision Cut Lung Slices

Precision cut lung slices (PCLS) are uniform lung tissues slices from animal models or human donors.³⁴ PCLS are valuable preclinical models that closely resemble intact lung architecture, cellular complexity, and mechanical properties beyond basic two-dimensional (2D) cell culture or three-dimensional (3D) tissue models. PCLS have multi-factorial purposes, such as pre-clinical investigation of VILI, cytokine assessments, mechanotransduction assays, and drug discovery (Figure 1).

Murine precision cut lung slices (mPCLS) can be readily generated to investigate the lung's microenvironment to optimize human respiratory health. Mice have genomes and immune responses similar to humans.²⁵ Additionally, mice mature quickly and can be genetically modified to assess specific mechanisms of lung disease development.⁴ Thus,

mPCLS provide preserved lung tissue structure, cellular interactions, and functional relevance generating *ex vivo* insights. However, there are also limitations of mice and mPCLS. Mice lack certain mechanotransduction pathways, breathe differently, and tolerate lung injury differently. mPCLS cannot achieve exact translatability in comparative medicine studies due to differences in lung sizes as well as physiological (i.e. total lung capacity) and anatomical (i.e. branching pattern) details.¹² Although there are limitations, mice and subsequently generated mPCLS remain a leading pre-clinical model of ALI. To account for these differences, our proposed methods will be readily extended to human PCLS (hPCLS).

When mPCLS were cryopreserved, cellular metabolic activity was somewhat reduced yet still within acceptable range. Additionally, mPCLS cryopreservation did not impact biological activity, such as airway contractility. Considering duration, cryopreserved mPCLS stored for greater than 2 weeks did not significantly affect viability.²⁸ Importantly, the PCLS can easily be subjected to experimental dynamic mechanical stretch – a key VILI-associated stimulus. To deliver cyclic, equibiaxial stretch that mimics mechanical ventilation, a multi-well PCLS stretcher was developed and validated. The high-throughput stretching system is capable of acute exposures under uniform cyclic stretching without compromising tissue viability.²²

To quantify tissue viability, a commercially available MTT ((3-(4,5-dimethylthiazol-2-yl)-2,5-diphenyltetrazolium bromide) assay was utilized. The MTT compound contains a tetrazolium ring reduced by mitochondrial dehydrogenases in active cells (Figure 2). MTT's water-soluble yellow dye was reduced to a blue formazan

product when cleaved by mitochondrial NAD(P)H dependent oxidoreductases. Viable cells internalized MTT and transformed into an insoluble blue formazan, which is further quantified and correlated to cell viability.

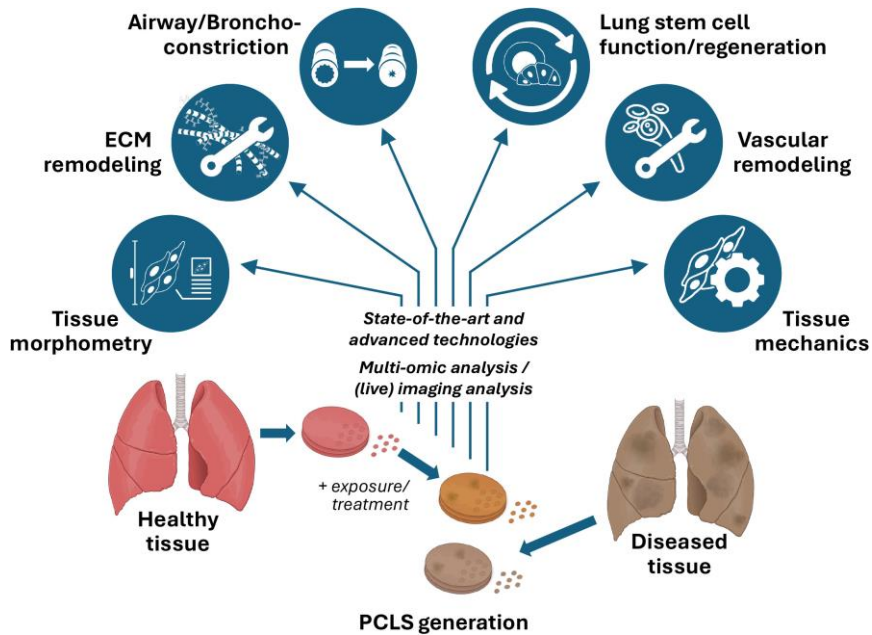


Figure 1. Schematic of the role of PCLS to study multi-factorial mechanisms of lung remodeling. Healthy versus diseased PCLS have the potential to generate translational insights on variable lung remodeling mechanisms from tissue mechanics to regenerative biology.¹⁸

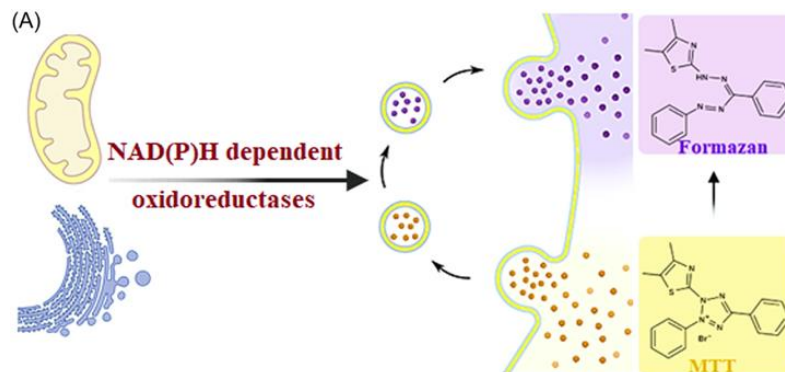


Figure 2. Schematic of MTT biochemical mechanism of action. Soluble yellow MTT was reduced to insoluble blue/purple formazan by mitochondrial NAD(P)H oxidoreductases transferring electrons.¹³

HYPOTHESIS

- 1) A model system can be optimized to cyclically stretch mPCLS over a 24 hour period, while preserving sterility and viability.
- 2) These experiments can be achieved in a 12-well format.

AIMS

Aim 1: Optimize a high throughput bioassay system for mPCLS membrane adherence and stretch.

- 1A) Establish and enhance mPCLS metabolic signal scope.

Aim 2: Assess the role of air blow, utilized adhesive, and cyclical stretch on mPCLS viability.

- 2A) Generate optimal air blow conditions to the stretcher membrane.
- 2B) Assess viability with and without NuSil® adhesive.
- 2B) Assess viability with and without cyclical stretch.

Aim 3: Quantify the effects of cyclical stretching on mPCLS adhesion and viability.

- 3A) With cyclical stretch, measure metabolic activity and image adhered mPCLS.

METHODS

Precision Cut Lung Slices

Figure 3 illustrated a schematic of PCLS preparation for mice (mPCLS). *Cdh2^{fl/+}*-*SMAA-Cre* mice were bred and maintained at the National Institute of Allergy and Infectious Diseases (Bethesda, MD) for use in our collaborator's (Kirk Druey) laboratory.²³ Mouse lung lobes were inflated with Hanks' Balanced Salt Solution (HBSS) and sectioned with a vibratome (VF-310-0Z, Precisionary Instruments LLC, Natick, MA) generating 250 μ m thick mPCLS. Once mPCLS were generated, there was a 3-6 day window from tissue harvest.²⁸ mPCLS were transferred to a 37°C incubator in Dulbecco's Mod. Of Eagle's Medium/Ham's F-12 50/50 Mix with L-glutamine and 15 mM HEPES (DMEM/F-12, Corning, Manassas, VA), changed every hour for the first 4 hours, and followed by a daily change.

mPCLS were also prepared and cryopreserved in the Druey laboratory. A subset of slices were cryopreserved and shipped to the Krishnan laboratory for our proposed studies. Specifically, PCLS were individually transferred to a cryovial containing 10% DMSO and DMEM/F-12 and placed into a Mr. Frosty Freezing Container in -80°C. After 24 hours, each cryovial was transferred to liquid nitrogen for longer storage or sent to the Krishnan laboratory for testing. When PCLS were needed for experiments, each cryovial was thawed in a 37°C water bath, carefully removed, washed in DMEM/F-12, and placed in a sterile 37°C incubator with 95-100% humidity and 5% CO₂ for up to 14 days.²⁸ Generally, *in vivo* experiments were completed within 3 days of mPCLS thaw (Figure 4).

In vivo experiments using live and cryopreserved PCLS were all conducted at the Research North Facility of Beth Israel Deaconess Medical Center (Boston, MA).

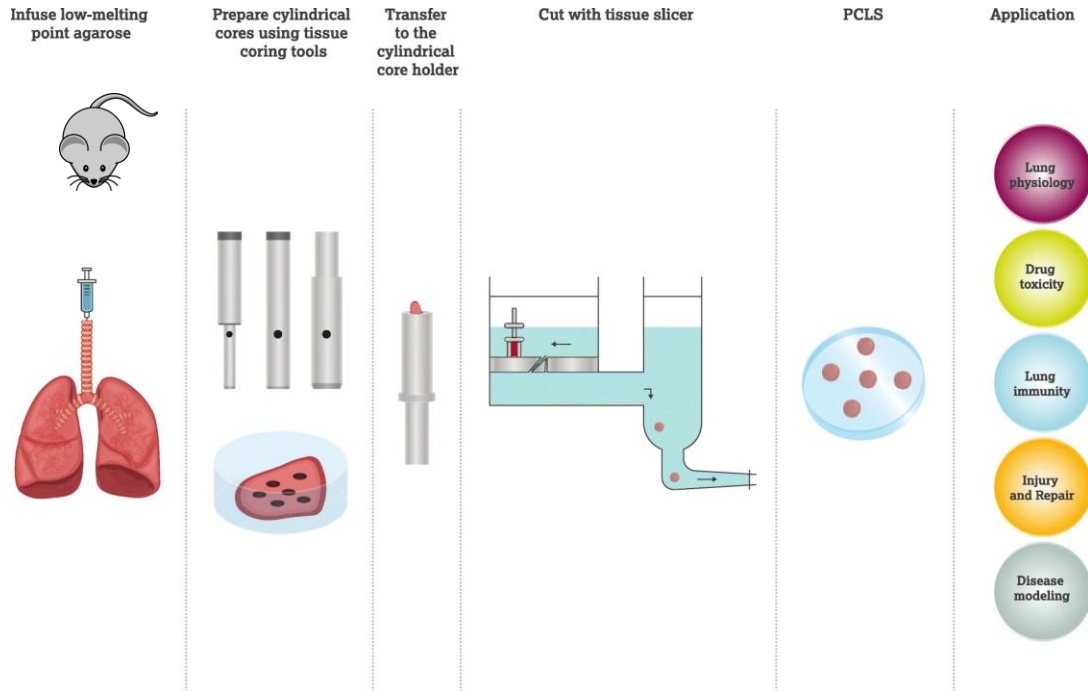


Figure 3. Schematic of PCLS workflow from harvest to application. Following tracheotomy, murine lungs are infused with agarose to maintain lung and airway structure and integrity, solidified lung samples are cored into cylindrical tissue components for tissue sectioning, sectioned with a vibratome to generate a precision cut lung slice approximately 100-500 μm thick, and can be utilized for multiple translational applications.²⁰

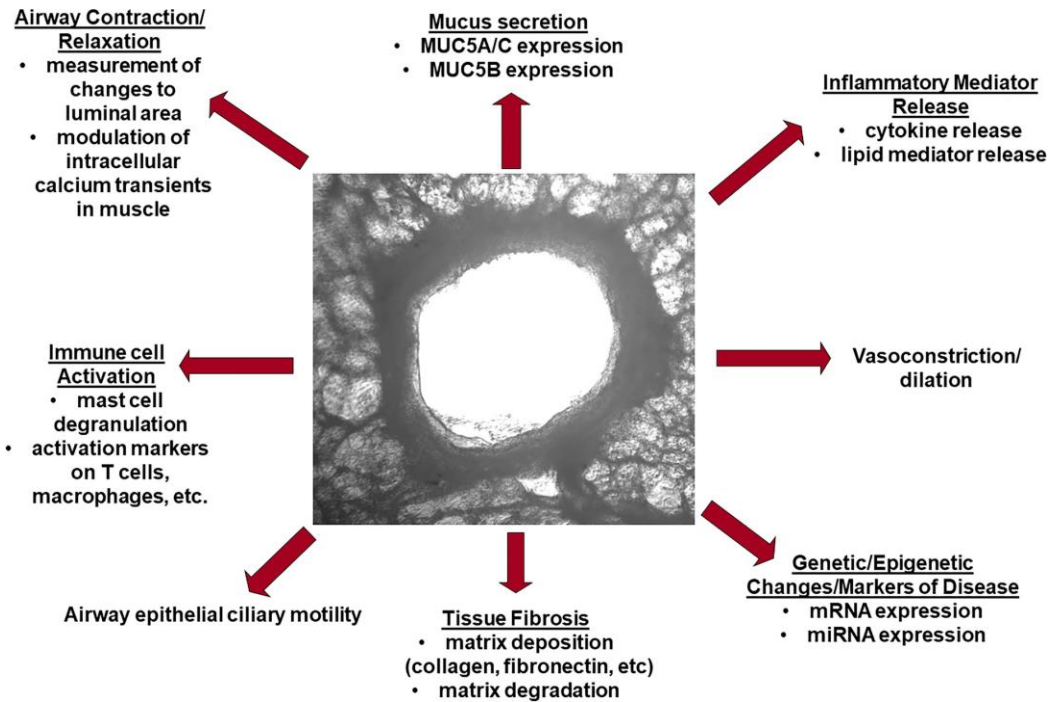


Figure 4. Schematic of different experiments involving a PCLS lung airway. By assessing anatomical airway responses in PCLS, biomechanics, inflammatory responses, pathological processes, and genetic biomarker expression can be investigated.¹⁵

Elastic Membrane Preparation

A custom-designed sticky elastic composite comprised of a stiff silicone bare membrane (Specialty Manufacturing Inc, .005” Silicone Sheeting) was coated with a 50 um thick layer of Gel-8100 (NuSil® Silicone Technologies, Carpinteria, CA). Gel-8100 was prepared as a 1:1 (Part A : Part B) mix and cured at 90°C for more than 1 hour. After curing, the composite had a Young’s Modulus of 0.36 kPa. A final top layer of Gel-8100 was prepared at a ratio of 1.15:1 (Part A : Part B) mix and cured at 90°C for more than 5 days to form a tacky, sticky layer sufficient for PCLS adhesion.^{26, 38} (Figure 5).

A custom-designed 6360 elastic composite comprised of a stiff silicone bare membrane was coated with a 50 μm thick layer of Gel-6360 (NuSil® Silicone Technologies, Carpinteria, CA). Gel-6360 was prepared as 1:1 (Part A : Part B) mix and cured 90°C for more than 1 hour. Gel-6360 was naturally tacky and allowed for adequate PCLS adhesion (Figure 5).

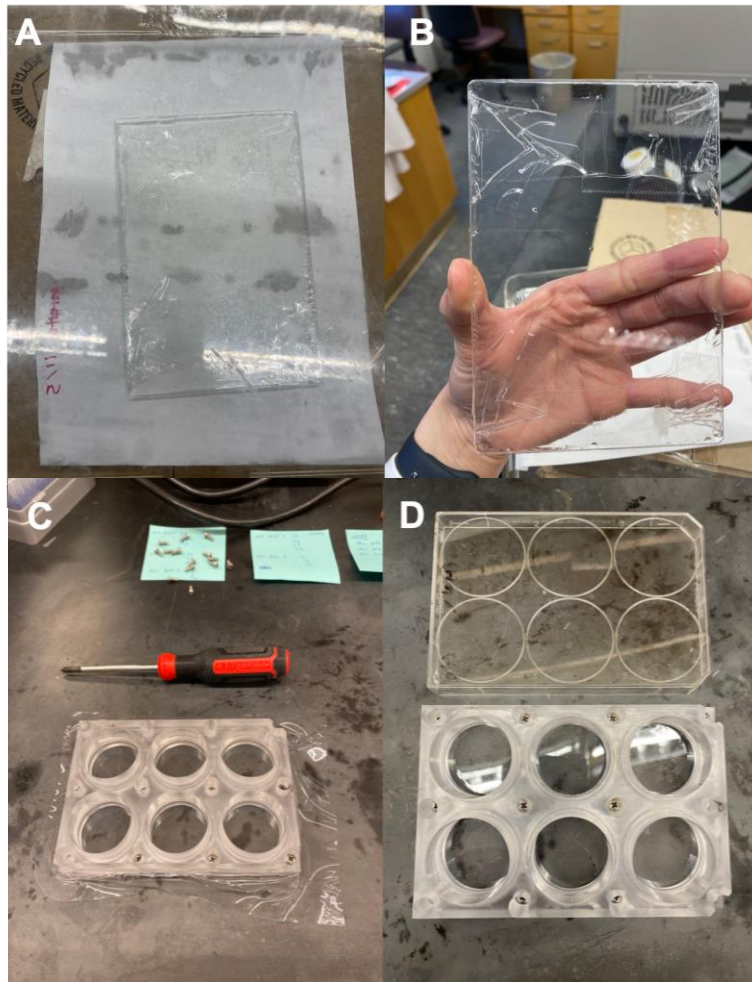


Figure 5. Customized elastic membrane and FlexFrame assembly. (A) Double layer sticky or 6360 elastic membrane was cured at 90°C for approximately 5-10 days. (B) Sticky side faced up. (C) Elastic membrane was positioned between the top and bottom pieces of a 6-well FlexFrame. 12 screws keep the membrane in position. (D) Excess elastic membrane edges are trimmed to match the FlexFrame perimeter and ready for experimental use.

NuSil® Adhesive

Med3-4213 fast-cure NuSil® silicone adhesive (Lot: 109401, Avantor, PA) was utilized to adhere mPCLS to the sticky membrane. Med3-42123 NuSil® adhesive was cured at room temperature (20°C) and rapidly cured with application of heat, such as in the incubator (37°C). To prepare the Med3-42123 NuSil® adhesive, two silicone-based components were mixed together (Part A + Part B) in a petri dish approximately 10 minutes before use. Part A was comprised of silanamine, 1,1,1-trimethyl-N-(trimethylsilyl), hydrolysis products with silica, and octamethylcyclotetrasiloxane. Part A appeared translucent and runny. Part B was comprised of silanamine, 1,1,1-trimethyl-N-(trimethylsilyl), siloxanes and silicones, dimethyl, methyl hydrogen, methyl vinylcyclosiloxane, and octamethylcyclotetrasiloxane. Part B appeared white, opaque, and viscous (Figure 6).

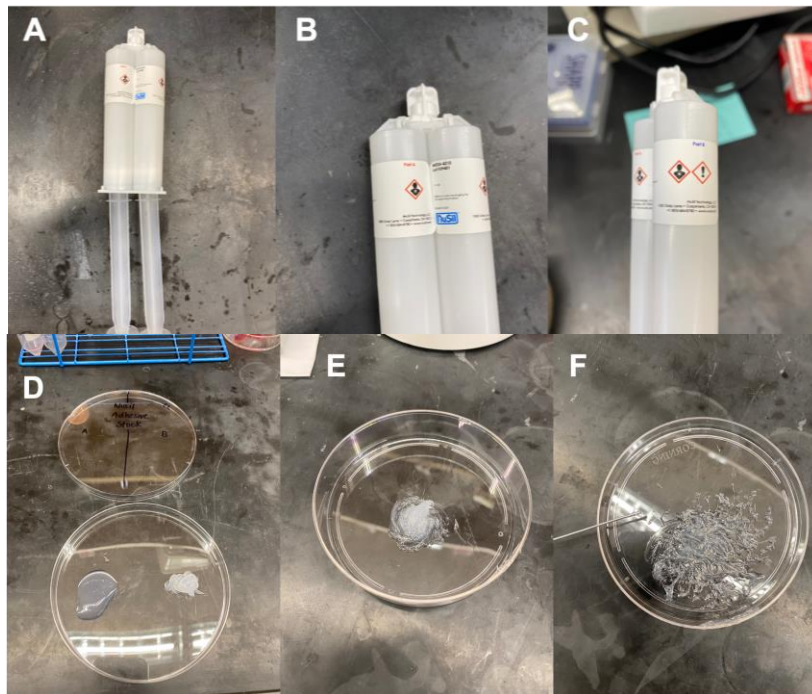


Figure 6. NuSil® adhesive preparation. (A) Med3-4213 fast-cure NuSil® silicone adhesive syringe applicator. (B-C) Part A and Part B silicone adhesive components. (D) To the left, translucent Part A displayed. To the right, opaque Part B displayed prior to being mixed together. (E) Part A + Part B mixed together to form a thick and tacky silicone-based adhesive. (F) Using the tip of a paper clip, the adhesive was carefully and meticulously applied to the perimeter of the mPCLS on the sticky membrane.

mPCLS Treatment

Thawed mPCLS were acclimated in 0% DMSO and 100% DMEM/F-12 for 24 hours in a sterile 37°C incubator with 95-100% humidity and 5% CO₂. 24 hours later, a subset of the thawed mPCLS were treated with 50% DMSO and 50% DMEM/F-12 as a positive control for zero viability (dead). Additionally, a subset of thawed mPCLS were stored in HBSS and placed in 4°C for minimum 1 week as a matched positive control for zero viability (certified dead).

Adhering and Plating mPCLS

A 500 uL bubble of sterile HBSS was placed in a well on top of the sticky membrane utilizing surface tension. Using an angled tweezer, mPCLS are transferred to the center of the HBSS bubble. A 1000 uL pipette was used to remove excess HBSS until the mPCLS sits in the center of well without completely drying out tissue. An air blower with a 4 mm inner tube diameter was set at 20 psi (~140 kPa) and placed approximately 3.4 cm above the mPCLS in the well for 20 seconds to ensure mPCLS was promptly attached to the sticky membrane (Figure 7). Using the tip of a paper clip, six dots of NuSil® adhesive are placed directly onto the sticky membrane surrounding the perimeter of the mPCLS. 3 mL of HBSS was used to rinse the well of any residual residue produced by the NuSil® adhesive followed by an additional 3 mL of HBSS to rehydrate

the mPCLS (Figure 8). After each of the FlexFrame's six wells are adhered and plated with mPCLS, the HBSS is replaced with 3 mL of DMEM-F12 in each well and placed overnight in the incubator (37°C) for the NuSil® adhesive to polymerize.

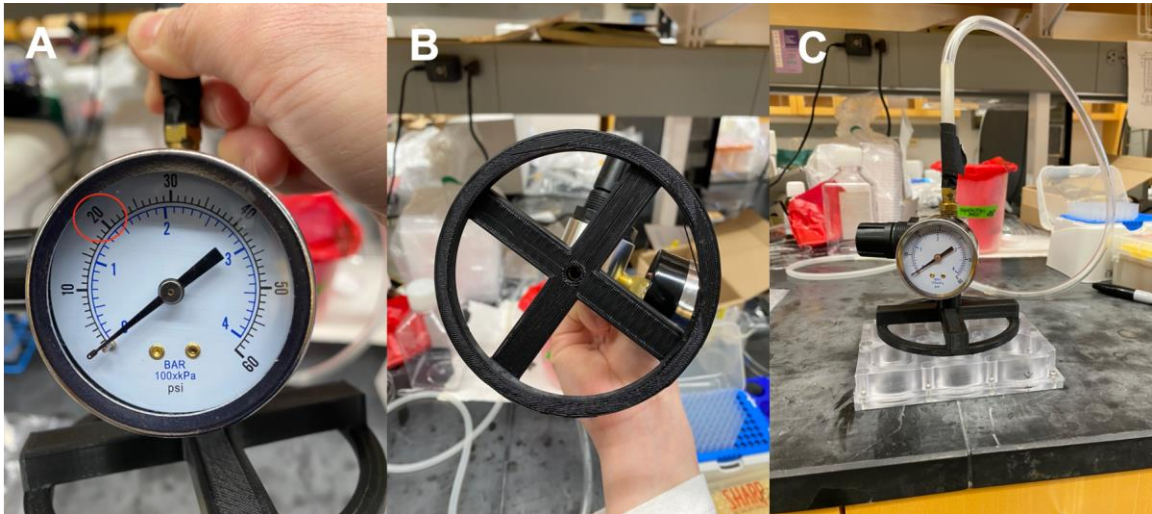


Figure 7. Experimental mPCLS were air blown at 20 psi for 20 seconds. (A) Air blow was set to 20 psi (~140 kPa) based on pressure gauge reading. (B) 4 mm inner tube diameter distributed air flow across the surface area of a single mPCLS. (C) Bench top air blower was positioned above a single well to adhere mPCLS to the elastic membrane prior to NuSil® adhesive application.

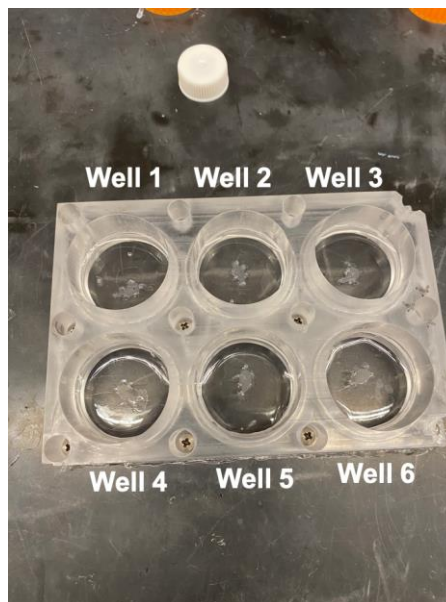


Figure 8. FlexFrame with adhered mPCLS on sticky elastic membrane (n=6) for cyclical stretching. mPCLS were transferred to a small amount of HBSS in the center of the well. mPCLS were subject to air blowing at 20 psi for 20 seconds. The small bubbles represent NuSil® adhesive dots around the perimeter of the mPCLS. The mPCLS were rinsed once with 3 mL of HBSS to remove excess oily residue from NuSil® adhesive. Each well contained a single adhered mPCLS and received fresh 3 mL of HBSS. Before transferring to the 37°C incubator, HBSS was replaced by 3 mL of DMEM/F-12 prior to cyclical stretching.

Multi-Well Stretcher

Figure 9 illustrated a multi-well stretching system with an actuating stage containing fixed indenter posts fitting up to two reusable, 6-well plate “FlexFrames.” The top and bottom components of the FlexFrame were separated to receive a customized disposable elastic, silicone membrane (Specialty Manufacturing, Inc.). The attached lung slices were positioned on the interchangeable sticky membrane with a silicone-based NuSil® adhesive (Avantor, PA) for cyclical stretching following the deformation of the membrane. Once the ball bearings were affixed to the indenter posts, the stretching system will move vertically with the linear motor. The bearings also reduce friction, thus heat-induced damage, and lag effect as the elastic membrane was stretched during the loading, stretching, and unloading process. As the stage moves down, the membrane with attached lung slice meets a fixed, cylindrical post that stretches the entire area of the well. Conversely, as the stage moves back up, the membrane with attached lung slice relaxed (Figure 9A, 9C) Figure 12 demonstrated the calibration data points generated by the multi-well stretcher prior to experimental use. Additionally, a custom software for the multi-well stretching system (Hecate cell stretcher program) allowed modifications of waveform, frequency, amplitude, and duration of cyclical stretching to create variable experimental conditions of interest (Figure 10C).

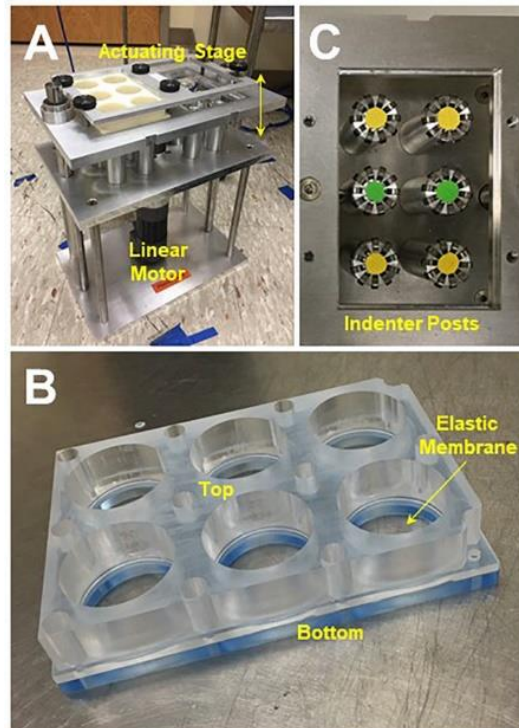


Figure 9. Mechanotransduction bioassay system components. (A) The multi-well device included 2 actuating stages where the assembled FlexFrame(s) were positioned. Additionally, the actuating stage is powered by a linear motor that moved the actuating stages up and down. (B) The reusable 6-well FlexFrame was customized to easily assemble interchangeable elastic membranes between a removable top and bottom component. (C) Looking down at the actuating stage, ball bearings were affixed to indenter posts minimizing friction during cyclical stretch of the assembled FlexFrame.²²

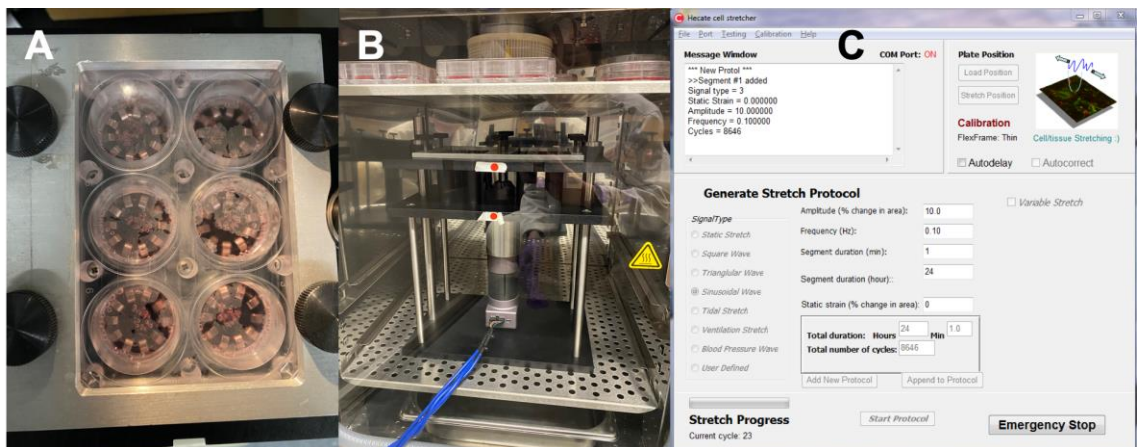
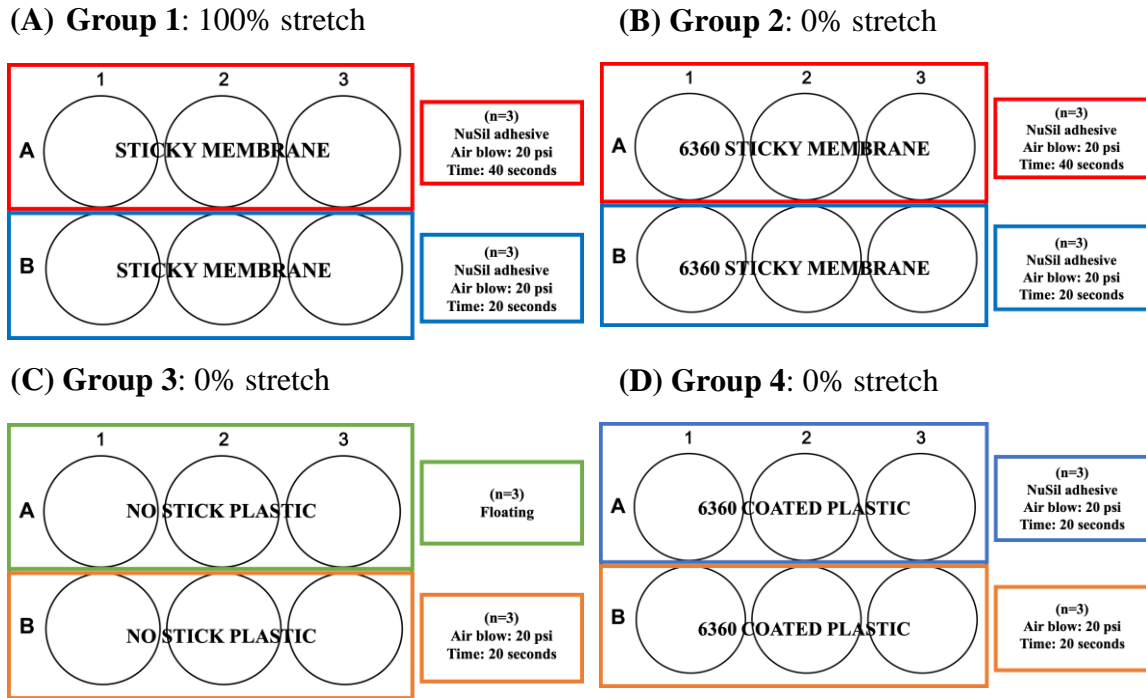


Figure 10. *In vitro* application of cyclical stretching on mPCLS. (A) Flexframe with adhered mPCLS in DMEM/F-12 (n=6) on sticky elastic membrane mounted to the right actuating stage. (B) Entire mechanotransduction assay system was sterilized with 70% ethanol and placed into sterile 37°C incubator for cyclical stretching. (C) Cyclical stretching protocol programmed on Hecate cell stretcher (Signal type: sinusoidal wave, Amplitude: 10%, Frequency: 0.1 Hertz (Hz), Duration: 24 hours, Static strain: 0%).

Setting Up Experimental Plate Conditions

Figure 11B-D represented the 0% stretch plates with varying coated membranes and mPCLS exposure conditions of interest (air blow, NuSil® adhesive, and floating controls). Without the addition of cyclical stretch, mPCLS were assessed for adhesion and viability.

After 24 hours of NuSil® adhesive polymerization in the incubator (37°C), individual mPCLS (n=6) were attached to the center of the sticky elastic membrane on the complete FlexFrame plate. Using the Hecate cell stretcher program, a FlexFrame plate was programmed to sinusoidal stretch conditions recapitulating mouse breathing for 24 hours in 37°C (Figure 10, Figure 11A). Following stretching, mPCLS were assessed for adhesion and viability.



Group	Plate Material	NuSil® adhesive	Air blow (20 psi)	Air blow time (sec)		Stretch
1	Sticky membrane	✓	✓	40	20	✓
2	6360 sticky membrane	✓	✓	40	20	
3	No stick plastic			None	20	
4	6360 coated plastic		✓	20		

Figure 11. Experimental conditions to evaluate adherence and viability. (A) **Group 1** served as the stretch experiment plate to evaluate sticky membrane conditions, NuSil® adhesive exposure, and identify optimal air blow conditions. In the future, this is the working model for PCLS stretch experiments. (B) **Group 2** served as the 0% stretch experiment plate to evaluate 6360 sticky membrane conditions, NuSil® adhesive exposure, and identify optimal air blow conditions. (C) **Group 3** served as the 0% stretch control plate with untreated mPCLS and mPCLS without NuSil® adhesive exposure and optimal air blow conditions. (D) **Group 4** served as the 0% stretch experimental plate to evaluate 6360 coating on a plastic plate, NuSil® adhesive exposure, and optimal air blow conditions.

Measuring Cell Viability

To measure the metabolic enzymatic activity of the mPCLS, a MTT assay was performed (Life Technologies Vybrant MTT Cell Proliferation Assay, Carlsbad, CA). mPCLS were incubated for 4 hours in HBSS containing 10 μ L of 12 mM MTT solution per well. Visually, viable mPCLS stained blue/purple. Absorbance of mPCLS, with and without supernatant, were measured at 570 nm.

Statistics

Statistical analyses for all in vitro studies were conducted with R software (Ver. 4.0.3). Raw data was uploaded into R software and statistical significance was determined with Student's t-test or one-way Analysis of Variance (ANOVA). Following ANOVAs, a Tukey Honest Significant Difference (HSD) post-hoc analysis was used to assess differences between pairs of groups. Statistical significance thresholds were * $p < 0.05$, ** $p < 0.01$, *** $p < 0.001$, **** $p < 0.0001$.

RESULTS

Verifying Stretch Calibration

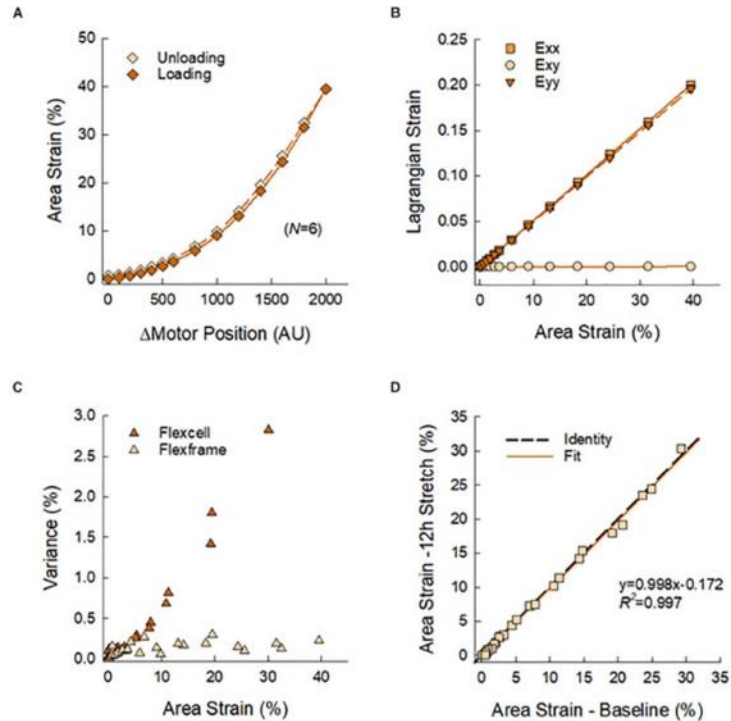


Figure 12. The working mechanotransduction bioassay system was calibrated prior to beginning stretch experiments. (A) Calibration curve relating change in motor position to area strain percentage. Each symbol represented the mean area strain of all 6 wells in a complete FlexFrame. (B) Comparable Exx and Eyy strains and negligible Exy area strain percentage. (C) The reusable FlexFrame exhibited low variance in area strain percentage. (D) After 12 hours of cyclical stretching, there was no mechanical change in elastic membrane strain.

Establishing mPCLS Adherence Conditions

A series of experiments were conducted to generate optimal mPCLS adherence conditions and summarized in a flow chart (Figure 13). We found that sticky membrane was the best material. Pre-washing NuSil® adhesive once in HBSS to remove oily residue before application negatively impacted the effective tackiness. Instead, NuSil® adhesive was rinsed with HBSS after application to the mPCLS perimeter in the FlexFrame well removing oily residue. Air blow at 20 psi for 20 seconds was sufficient to promptly adhere the mPCLS to the sticky membrane without completely drying out the tissue.

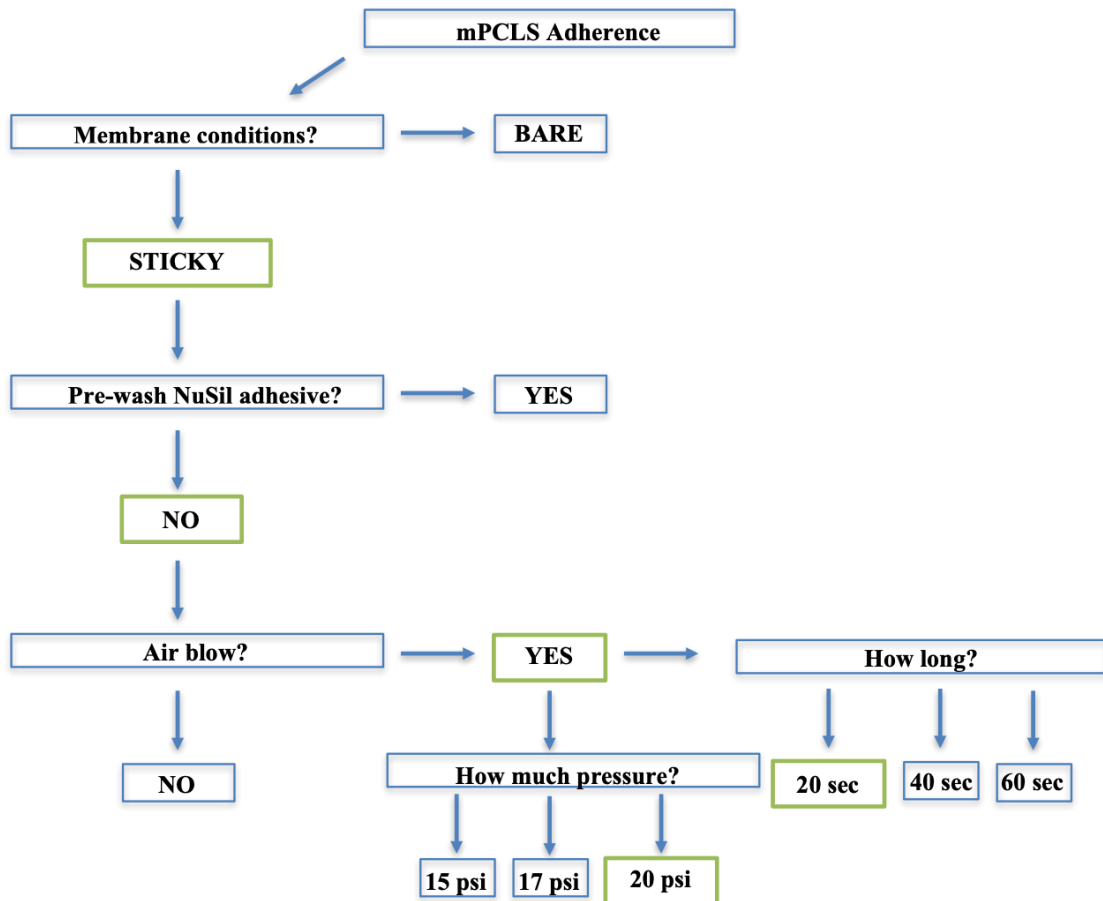


Figure 13. Flowchart detailing the workflow of optimizing PCLS adherence. Each aspect of the PCLS adherence protocol was carefully modified to achieve optimal conditions for FlexFrame plating. These optimized conditions included using a fresh sticky membrane with air blown lung tissue (20 psi for 20 seconds) reinforced with NuSil® adhesive. The FlexFrame was incubated overnight and followed by cyclical stretching, adherence validation, and viability quantification.

Enhancing mPCLS Metabolic Signal Scope

To measure metabolic enzymatic activity of mPCLS, a customized MTT assay protocol was developed and adapted from a working cell culture protocol. As seen in Figure 14, active hASM cells were seeded at a range of densities (5K to 40K) to confirm the MTT reagent was working properly and quantify an expected signal scope of viability. Additionally, incubation times from 4 to 24 hours were investigated given hASM cells actively multiply in DMEM-F-12 culture media, while mPCLS were tissue-based samples. The primary goal was to incubate for the least amount of time without compromising viability measurements to generate a sustainable MTT assay for mPCLS use.

According to Figure 14, 4 hours of incubation was sufficient to establish a signal scope between serial cell seeding densities. Although 24 hours showed the greatest absorbance at 40K cell seeding density, this may be attributed to active cell growth overnight rather than provide a standard viability measurement, like the mPCLS should. Across 5K to 20K cell seeding densities at 24 hours, the signal scope was comparable to 4 hours. Previously, the working cell culture MTT protocol utilized hydrochloric acid (HCl) treatment after MTT incubation. However, after several validating mPCLS experiments, Figure 15 demonstrated that it was not necessary for sufficient tissue absorbance reading. Additionally, 4 hours of mPCLS MTT incubation was ideal to

achieve quantifiable results. Of note, MTT visually stained the mPCLS blue/purple resulting in correlated absorbance readings when tissue and supernatant were measured together on the Biotek Cytation 1 Cell Imaging Multi-Mode Reader (Agilent Technologies, Lexington, MA) at 570 nm.

According to Figure 16, there was no significant difference in absorbance plate readings between wet versus dry samples. Figure 17 demonstrated the effort to establish baseline signal scopes of the MTT assay. Among treatment conditions, untreated mPCLS served as the negative control for viability, while 24 hours of DMSO-treated mPCLS served as the positive control for no viability. Fold change was calculated for 5 experimental conditions treated with and without 4 hours of MTT incubation. When treated with MTT, mPCLS achieved approximately a 4-fold increase compared to untreated mPCLS. Additionally, when treated with MTT, mPCLS achieved approximately a 2.5-fold increase compared to DMSO-treated mPCLS (no viability).

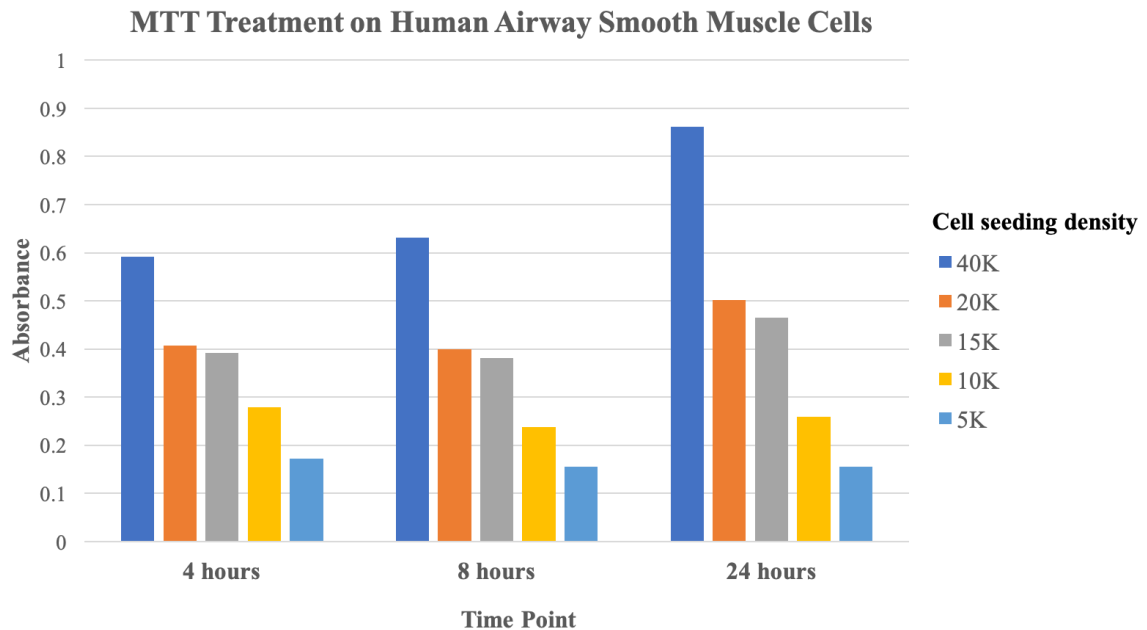


Figure 14. MTT assay was successfully validated on actively cultured human airway smooth muscle (hASM) cells. After 4, 8, and 24 hours of MTT treatment, absorbance values were measured at 570 nm. As expected, hASM cells with the highest seeding density (40K) had the greatest viability, while lowest seeding density (5K) had the lowest viability. Additionally, 4 hours of incubation was sufficient to demonstrate scope of viability between varying cell seeding densities.

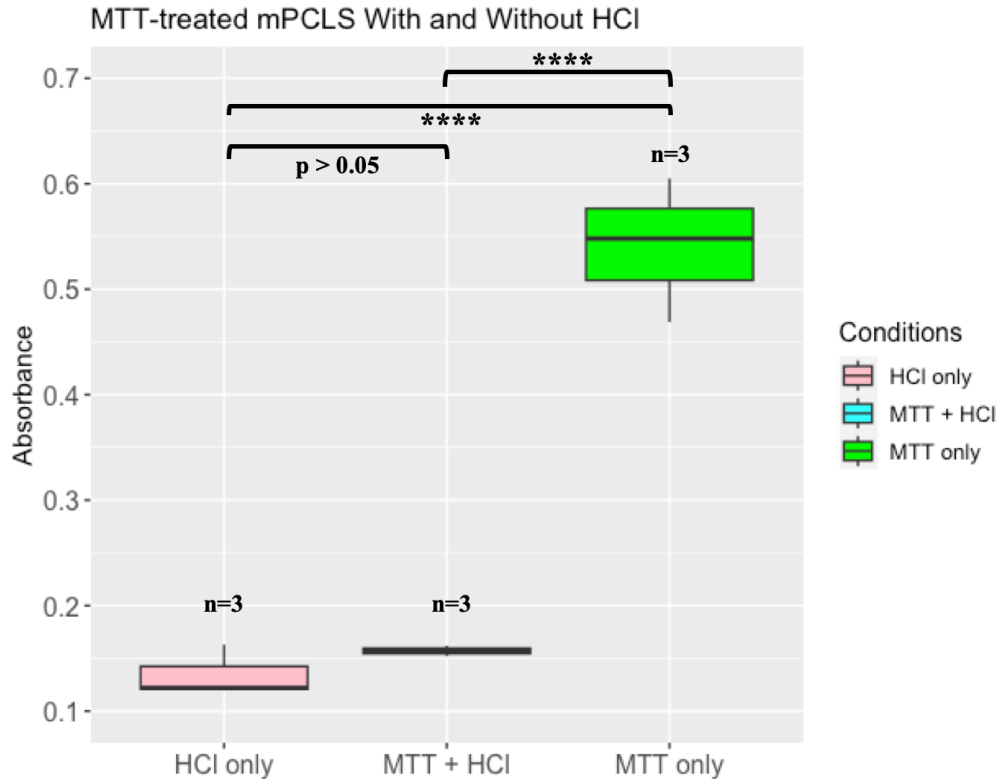


Figure 15. HCl is not necessary to optimize viability measurement in MTT-treated mPCLS. To establish the MTT assay protocol, mPCLS were treated with MTT + HCl, MTT only, or HCl only for 4 hours to evaluate absorbance values at 570 nm. MTT only, without HCl addition, resulted in the greatest average absorbance. There was no significant difference ($p > 0.05$) in absorbance values between HCl only and MTT + HCl. There was a significant difference ($p < 0.05$) in absorbance values between MTT only and both HCl only and MTT + HCl. **** $p < 0.0001$.

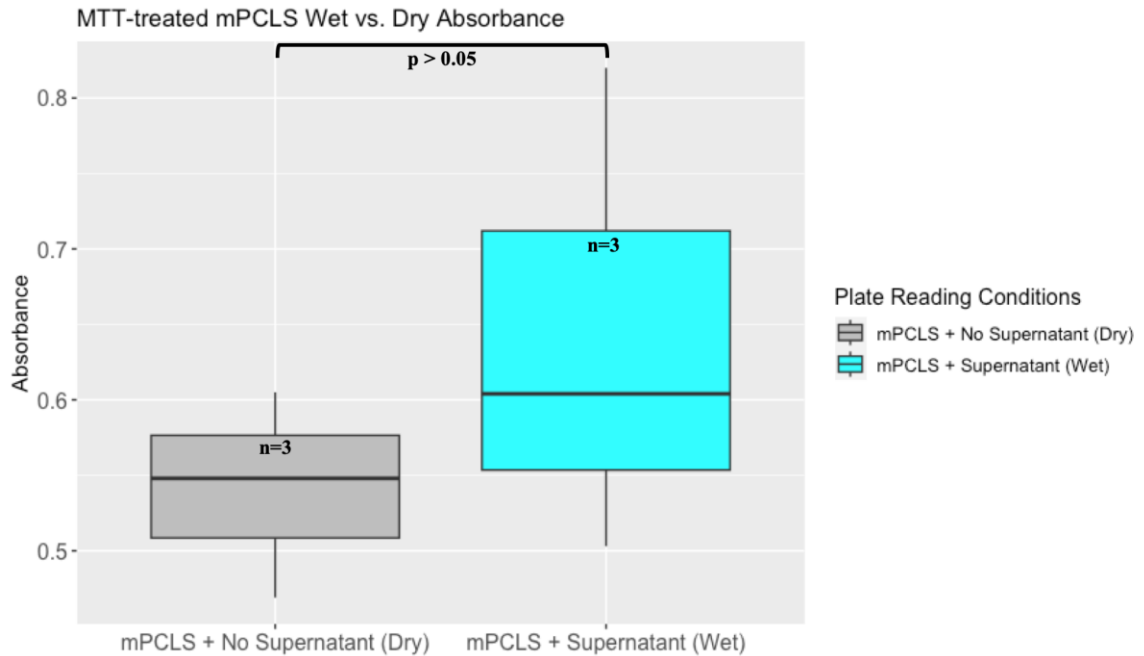


Figure 16. The absorbance of MTT-treated mPCLS measured with and without supernatant were not significantly different. To further establish the MTT assay protocol, the absorbance of MTT-treated mPCLS after 4 hours, with and without supernatant, were measured at 570 nm. There was no significant difference ($p > 0.05$) between average absorbance when comparing measuring mPCLS with supernatant (wet) compared to measuring the mPCLS alone without supernatant (dry). However, when reading the plate under dry conditions, mPCLS were more easily evenly distributed across the bottom of the plate.

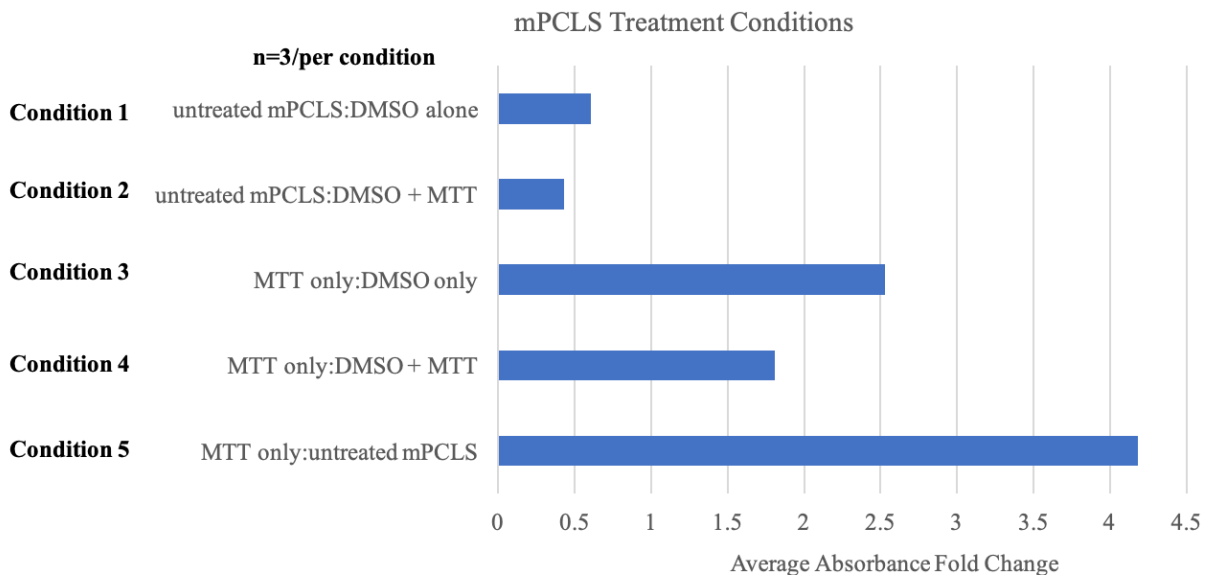


Figure 17. MTT-treated mPCLS demonstrated measurable signal scope validating adaption of MTT assay to tissue. 4 hours of MTT versus no MTT treatment were applied to different mPCLS exposure conditions (in triplicates) including untreated mPCLS (negative control) and DMSO-treated mPCLS (positive control). Average absorbance fold change between MTT versus no MTT treated mPCLS by exposure were measured at 570 nm to determine signal scope of MTT assay. In condition 5, MTT-treated mPCLS versus untreated mPCLS resulted in a 4-fold viability increase for MTT-treated mPCLS validating the MTT assay's function. In condition 3, MTT-treated mPCLS versus DMSO-treated mPCLS resulted in a 2.5-fold viability increase viability for MTT-treated mPCLS validating the working positive control of DMSO-treated mPCLS (no viability).

Quantifying Viability After Adherence

In order to quantify viability after optimal adherence conditions were established, we wanted to confirm the NuSil® adhesive and oily residue did not significantly impact metabolic activity. As a comparison, we also wanted to assess whether doubling air blowing time at 20 psi could improve mPCLS adherence and quantify any viability changes given the possible risk of drying out the tissue. As seen in Figure 18, NuSil® adhesive exposure and air blowing did not affect metabolic activity. When the air blowing exposure time was doubled, the absorbance readings became even more inconsistent suggesting more dry tissue risked viability.

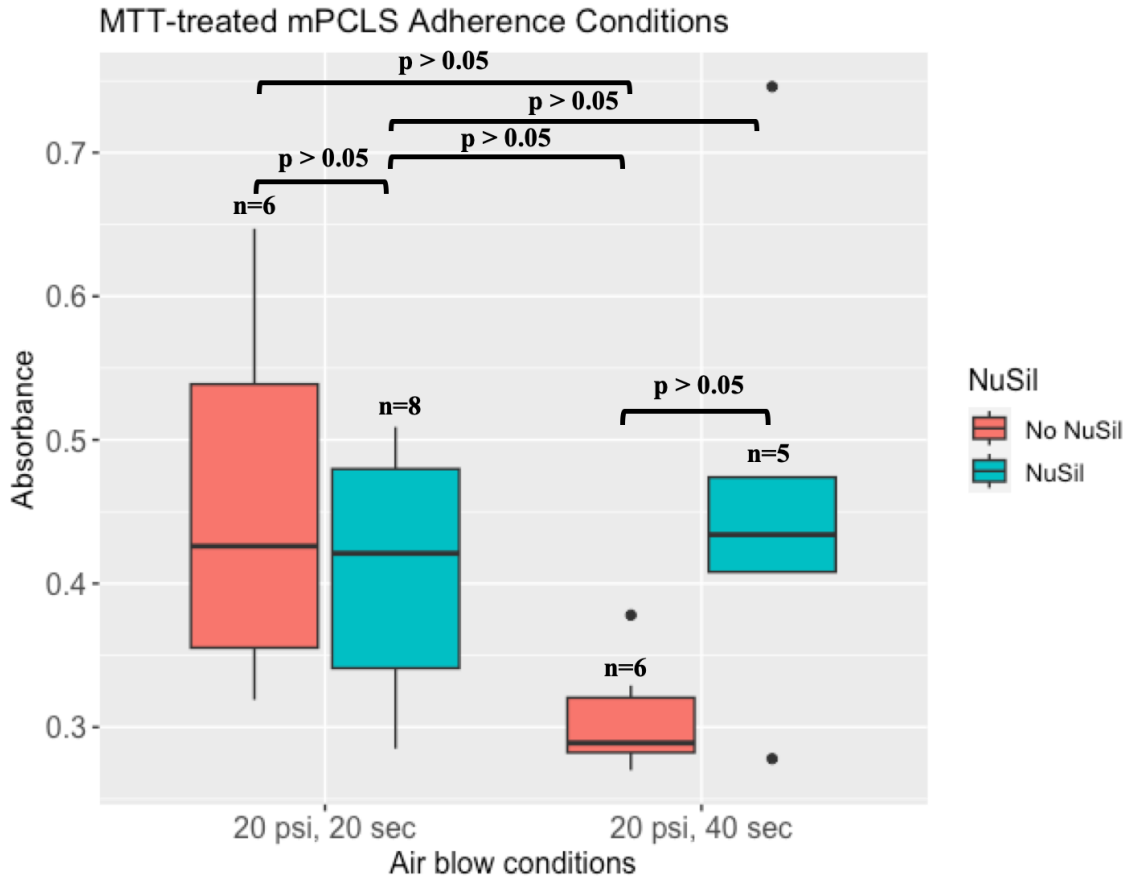


Figure 18. mPCLS adherence with NuSil® and air blow does not compromise viability. Optimal air blowing conditions were 20 psi at 20 seconds with comparable viability with and without NuSil® exposure. Air blowing at 20 psi at 40 seconds resulted in variable absorbance readings with higher viability in NuSil® exposed mPCLS.

Visualizing and Quantifying Adhesion

mPCLS were adhered to a sticky elastic membrane between a 6-well FlexFrame.

Using the multi-well stretcher, the mPCLS were subject to two protocols. Protocol 1 was a low magnitude stretch, while Protocol 2 was a high magnitude stretch. Serial images were captured without stretch, maximum stretch, and after stretch. Area was manually traced and measured with ImageJ software (National Institutes of Health, Bethesda, MD) (Figure 19). After protocol 1, the mPCLS demonstrated a change in area strain

([maximum stretch – no stretch]/[no stretch]*100) of 5.2% (Figure 20). After protocol 2, the mPCLS demonstrated a change in area strain of 10.8% (Figure 20). Change in area strain was the measured strain reproducible between stretch cycles. These differences between area strain reflect additive effects of adhesive layer thickness and PCLS thickness. Ongoing work is also ascertaining reproducibility between wells of the multi-well plate as well as between plates.

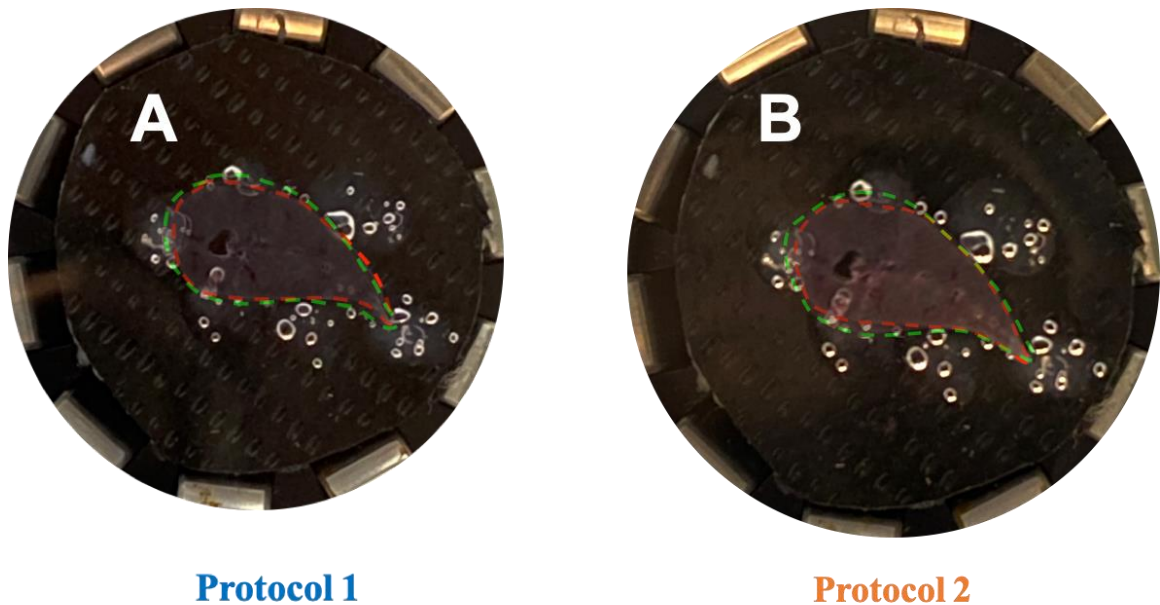


Figure 19. Adhered mPCLS were stretched at customized parameters. Red dotted lines represented the area of the mPCLS without stretch, while green dotted lines represented the area of the mPCLS at maximum stretch (A) Protocol 1 resulted in a 5.2% change in area between baseline (no stretch) and maximum stretch. (B) Protocol 2 resulted in 10.8% change in area between baseline (no stretch) and maximum stretch.

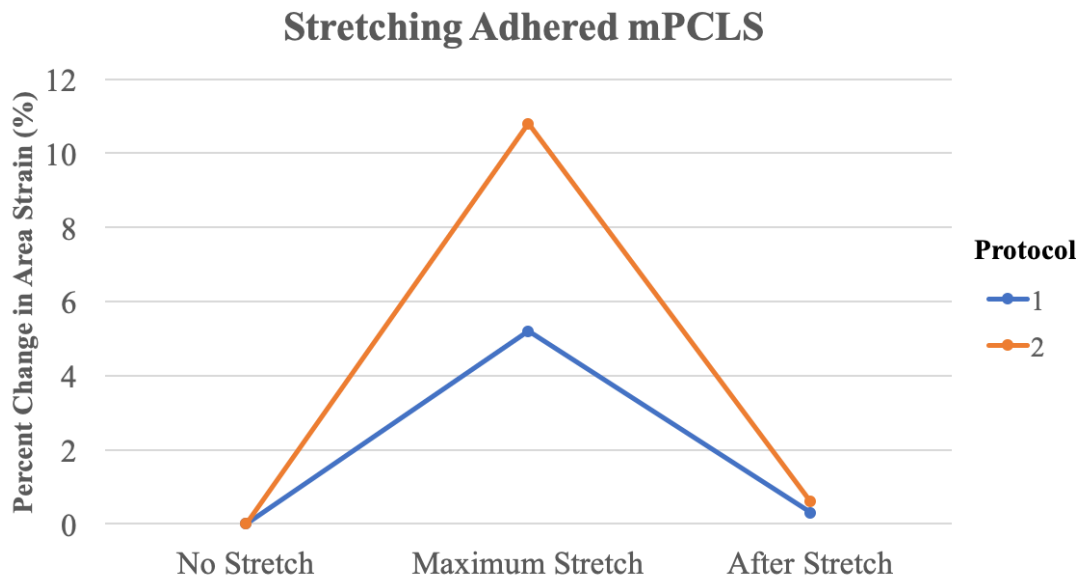


Figure 20. Adhered mPCLS demonstrated a direct relationship with stretch and percent change in area strain. The same mPCLS experienced near doubling of stretch, from protocol 1's low stretch to protocol 2's high stretch parameters, resulting in doubling of percent change in linear stretch between baseline (no stretch) and maximum mPCLS stretch conditions. After high stretch, the mPCLS had a slightly greater percent change in linear stretch between maximum and after stretch conditions.

Quantifying Viability

According to Figure 21, mPCLS in Group A experienced 24 hours of cyclical stretching. At 37°C, the NuSil® adhesive polymerize to ideally enhance mPCLS adherence. During preparation, mPCLS in A1 was not adhered in the center resulting in detachment after 24 hours of stretching likely from the indenter post creating positional strain on a top side of the mPCLS. Sturdy mPCLS in A2 and B2 were centered on the sticky membrane. Thus, the indenter posts were adequately positioned to deliver equibaxial stretch to the adhered mPCLS. mPCLS in A3 and B1 were centered on the sticky membrane. However, perimeter NuSil® adhesive dot placement may not have been in proximal contact with mPCLS causing partial adherence.

According to Figure 22, mPCLS were subject to the full spectrum of optimal adhesive conditions and cyclical stretching for the high-throughput mechanotransduction bioassay system we sought to optimize. Under stretching conditions, mPCLS had comparable viability absorbance to negative control mPCLS (no exposure) without statistical significance. As expected, the DMSO-exposed mPCLS (positive control) and “certified-dead” mPCLS (secondary positive control) had statistically significant lower viability absorbance compared to negative control and stretched mPCLS.

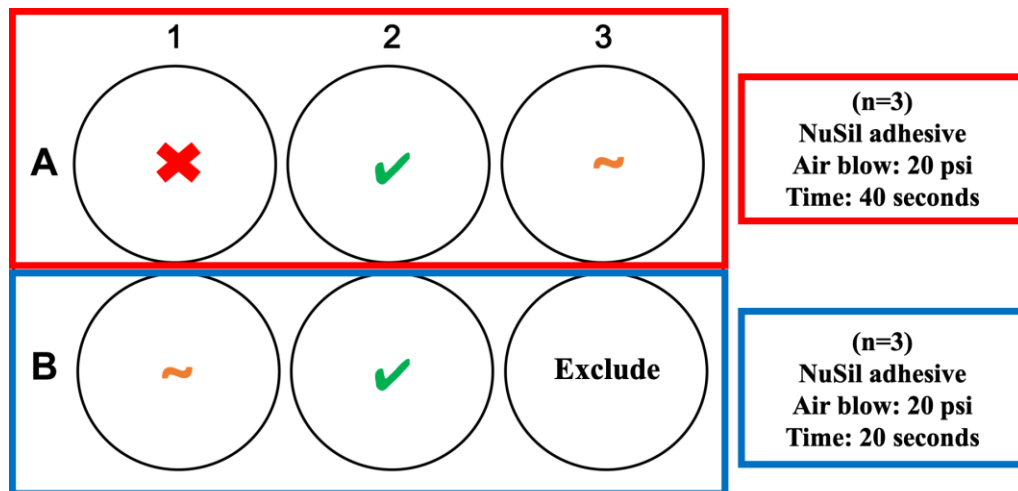


Figure 21. 4/6 mPCLS were adhered or partially adhered after 24 hours of cyclical stretching. In the Group A stretched FlexFrame condition, mPCLS were either detached (X), adhered (✓), partially adhered (~), or excluded after stretching overnight. mPCLS in wells A1-A3 were subject to NuSil® adhesive exposure and air blowing at 40 seconds (double the time). mPCLS in wells B1-B3 were subject to NuSil® adhesive exposure and air blowing at 20 seconds. Well B3 was excluded due to possible contamination confirmed by visually murky DMEM/F-12 media and an outlier high MTT absorbance reading.

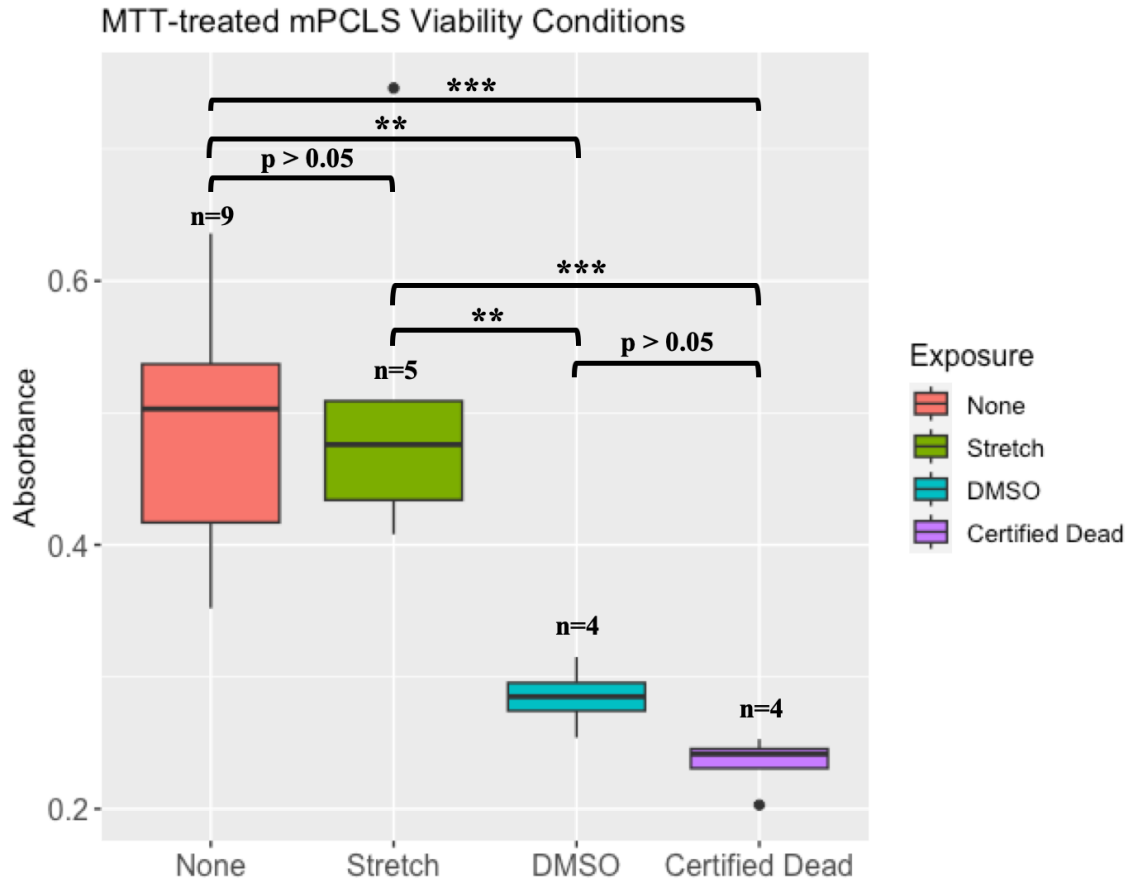


Figure 22. Cyclical stretching of mPCLS does not affect viability. Compared to control mPCLS (None), mPCLS that were cyclically stretched for 24 hours in a sterile 37°C incubator showed no significant difference in absorbance readings. As expected, DMSO treated and certified dead mPCLS (1 week in 4°C) had significantly lower viability compared to living mPCLS. ** $p < 0.01$. *** $p < 0.001$.

DISCUSSION

ARDS encompasses multi-factorial anatomical, physiological, and immunological mechanisms of ALI from alveolar epithelium damage, hypoxia from ventilation-perfusion mismatching, and infiltration of inflammatory cells with increased fluid permeability. To manage ARDS symptoms, mechanical ventilation is the mainstay respiratory therapy option. Despite the intentions to oxygenate critically ill patients, VILI is a major risk due to over-distention of alveoli (volutrauma), excessive pressure inflicted on working alveoli leading to overall lung over-distention (barotrauma), constant opening and collapsing of alveoli (atelectotrauma), and pulmonary inflammation (biotrauma)³⁵ (Figure 23).

Current treatments for acute respiratory failure in ARDS include careful management of driving pressure to overcome the positive pressure introduced with mechanical ventilation and prone positioning to improve oxygenation. Furthermore, there are no medical treatments for mitigating VILI-associated symptoms. This is an enticing opportunity to better understand VILI mechanisms to identify possible predictors that identify risk for VILI, such as driving pressure and mechanical power.² The driving pressure is derived from $P_{plat} - PEEP$, while mechanical power refers to the amount of energy via ventilator to respiratory system over time.^{35, 39} Additionally, there are future opportunities to develop possible pharmaceutical agents to alter biochemical targets to promote lung-protective mechanisms.

Real-time *in vivo* murine and human studies to investigate VILI and modification of mechanical power parameters are not feasible and ethical. Given the broad

complexities of VILI, PCLS are a valuable pre-clinical research model to explore targeted mechanical, biological, and pharmacological responses to cyclical stretch. PCLS can be utilized to explore mechanical manipulation and the role of pharmaceutical agonists or antagonists on VILI mechanisms. Furthermore, PCLS are practical given their ability to be cryopreserved while maintaining structural integrity, quantification of traction movement, and qualitative high-resolution imaging.¹⁴

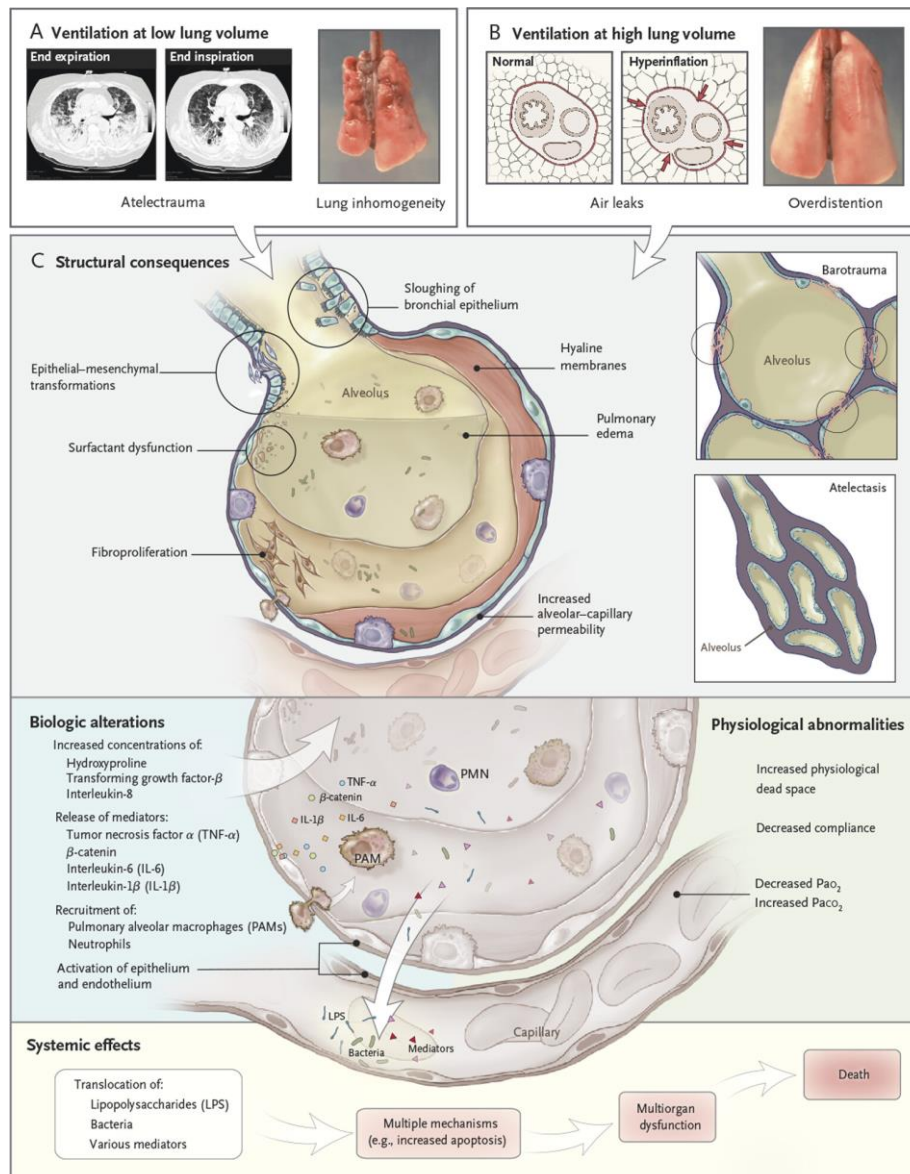


Figure 23. Schematic of atelectrauma, volutrauma, barotrauma, and biotrauma on the macroscopic lung and alveolar microenvironment. (A) Constant opening and closing of the alveoli creates inconsistency in the lung architecture homogeneity. (B) Excessive pressure causes overall over-distension of the lung causing air leakages, pulmonary edema, and increased permeability of the alveolar-capillary interface. (C-D) Biological and physiological alternations, such as pro-inflammatory cytokine release and immune cell infiltration and increased arterial carbon dioxide presence contributes to overall systemic dysfunction.³¹

Our lab has demonstrated a multiscale approach to apply stretch and measure the stiffness of PCLS adhered to an elastic membrane under equibaxial stretch.^{14, 22} We set out to optimize feasible aspects of the established *in vitro* mechanotransduction methodology that could be controlled to enhance reproducibility of PCLS studies. There were two important properties to critically assess: PCLS adherence and viability. The two driving principles of this critical assessment were to maintain a high-throughput environment that is biomechanically similar to the *in vivo* ventilated lung and generate quantitative and qualitative outputs to demonstrate viable biomechanical activity. The current adherence protocol used a fast-acting adhesive (Gorilla Super Glue, The Gorilla Glue Company, Cincinnati, Ohio) comprised of ethyl cyanoacrylate. Upon contact with liquid or alkaline substances, rapid polymerization occurs. However, this fast-acting adhesive released toxic byproducts and residues that ultimately impaired PCLS biochemical activity and viability.

Using cryopreserved mPCLS, we investigated the introduction of a new silicone-based adhesive (NuSil®) with tightly regulated air blowing parameters to demonstrate comparable adherence and enhanced tissue viability under mechanical stretch. Previously, our lab has demonstrated metabolic activity at 0, 2, and 6 hours after thawing was maintained in cryopreserved mPCLS.³⁶ Among cryopreserved mPCLS, the primary

goal was to incubate mPCLS with MTT for the least amount of time without compromising viability measurements to generate a sustainable protocol for future use. Our new MTT protocol was established from adopting a cell-cultured based protocol. Validating experiments were conducted on actively dividing hASM cells to establish a baseline signal scope of the MTT assay and determine a 4-hour incubation time. Once established, baseline signal scope of mPCLS viability were necessary to investigate unknown variables of interest, like NuSil® adhesive and air blow exposure, in the setting of cyclical stretch at 37°C (average body temperature).

A series of mPCLS treatment conditions followed by MTT assay experiments were conducted. An overall observation was that mPCLS had inter-variability sample to sample. This inter-variability was attributed to differences in mPCLS sizing and plate orientation when suspended in liquid. To account for these differences, a minimum of triplicates was included per exposure condition and wet (mPCLS + supernatant) versus dry (mPCLS + no supernatant) absorbance readings were collected to compare values revealing no significant difference in absorbance readings (Figure 16).

When treated with MTT, mPCLS achieved approximately a 2.5-fold increase compared to DMSO-treated mPCLS (no viability positive control). This was approximately a 2-fold decrease compared to untreated mPCLS (viable negative control). Intuitively, we expected the DMSO-treated mPCLS to yield an even greater fold change increase (greater than 4-fold). However, DMSO may interact with MTT diluting the intended fold change. Regardless of this possible interaction, every experiment where DMSO-treated mPCLS was used as a comparative positive control generated a

quantitative signal scope that was significantly different from untreated and experimental mPCLS. Furthermore, to account for this, we introduced a “certified dead” mPCLS validation group consisting of mPCLS in 4°C for approximately 1 week to ensure no viability. According to Figure 22, these “certified-dead” mPCLS were not exposed to DMSO and revealed minimal absorbance readings that were not statistically different from DMSO absorbance readings.

We generated a NuSil® with air blow adhesive protocol for future human and murine PCLS mechanobiology assays. Previously, the fast-acting Gorilla Super Glue released toxic byproducts that impaired viability and was no longer a sustainable adhesive. The silicon-based NuSil® adhesive was chosen because it matched the second composite layer of the customized elastic membranes generated in our lab.²⁶ From our past mechanotransduction assays, PCLS were subject to air blow at 2 psi (~14 kPa) for 1 minute.¹⁴ To further optimize, our primary goal was to ensure prompt adhesion of tissue to the membrane surface without completely drying tissue out and risking loss of viability. We opted to increase the pressure to 20 psi (~140 kPa) for less than 1 minute duration (20 seconds versus 40 seconds).

Figure 18 demonstrated the testing and quantifying of adherence with optimized air blow conditions and NuSil® adhesive exposure. When NuSil® adhesive dots were placed around the air blown mPCLS, an unknown oily residue was visualized when HBSS was added. We decided to rinse with HBSS once to discard the oily residue followed by rehydration with fresh HBSS and sterile DMEM-F12 prior to incubation to sustain tissue viability. The oily residue may be a byproduct of either Part A or Part B of

the NuSil® adhesive contacting liquid. With a single rinse of HBSS to remove some of the oily residue, there were no statistical differences in viability among mPCLS that were not exposed to NuSil® adhesive. Given these promising results, we elected to keep the single HBSS rinse of the mPCLS surrounded by NuSil® adhesive. Additionally, by increasing the air blow pressure (20 psi ~ 140 kPa) and decreasing exposure time (20 seconds), we did not compromise tissue viability.

To confirm mPCLS were adhered to the NuSil®-coated membrane and capable of customized stretching parameters, mPCLS were subject to a low or high stretch protocol. Qualitative serial images were taken at no stretch, maximum stretch, and after stretch to visually observe tissue expansion and contraction (Figure 19). Quantitatively, area was measured from the serial images to determine the percent change in linear stretch between the mPCLS without and at maximum stretch. As expected, there was a doubling of percent change in linear stretch between low and high stretch protocols confirming a direct relationship between equibaxial elongation and linear stretch (Figure 20). Particularly, during the high stretch protocol, there was an observed partial detachment at the southern tip of the crescent-shaped mPCLS. As a result of the partial detachment, the camera may have not captured the full mPCLS expansion at maximum stretch. In the future, exposing the adhered mPCLS with NuSil® adhesive for 24 hours in the 37°C incubator to polymerize the adhesive may prevent partial detachment at high stretch protocols.

To recapitulate *in vivo* mechanical ventilation, the optimized mechanotransduction bioassay system was subject to cyclical stretching (sinusoidal

wave) for 24 hours at 37°C (Figure 9C). The customizable Hecate cell stretcher program represented the ability to modify the settings of a mechanical ventilator based on a patient's respiratory needs. Our amplitude was set to 10% representing a low tidal volume. Tidal volume is the amount of air that moves in and out of the lung during the process of inhaling and exhaling. With mechanical ventilation management for ARDS, lung-protective strategies include pursuit of low tidal volumes.⁹ The frequency was set to 0.10 Hz (0.1 cycles per second, 6 cycles per minute). Given the use of mPCLS, we matched the average respiratory rate of mice. For hPCLS, the frequency can be set to 0.25 Hz (0.25 cycles per second, 15 cycles per minute).

Based on Figure 21, 4/6 mPCLS remained fully or partially adhered after 24 hours of cyclical stretching at 37°C. While hPCLS have a heavier, more robust, and convenient round shape, mPCLS are thinner, lighter, and have a crescent shape that impacted the perfect application of equidistant NuSil® adhesive dots. As this was the first trial of our optimized *in vitro* system, there is opportunity to work through these nuances. The most important pursuits for this first trial was the successful adherence and quantifiable viability measurement of at least 1 mPCLS. Not only did we achieve this, but we gained valuable data points confirming stretched mPCLS did not have statistically significant differences in viability when compared to control mPCLS. This gave us reassurance that our baseline stretching parameters did not affect viability. Furthermore, our encouraging data demonstrated the potential to investigate dynamic stretching parameters to model severe VILI and gain greater insights into other lung diseases.

CONCLUSION

Our broader clinical objective was to model *in vivo* VILI that critically ill patients with ARDS experience. We aimed to optimize an *in vitro* high-throughput bioassay system for mechanical stretch studies. Our fundamental hypothesis centered around gaining insights on PCLS adherence and viability under cyclical stretching. We proposed a new silicone-based adhesive, NuSil®, that shared similar properties with our custom elastic membranes would preserve tissue viability unlike the previous fast-acting Super Glue. Additionally, we strived to standardize air blowing pressures and exposure time testing greater pressures with less exposure time to prevent precious lung tissue from drying out and quantifying baseline metabolic activity signal scopes.

Our foundational work highlighted important findings that will propel future PCLS studies in our lab: (1) Metabolic enzyme activity of mPCLS was easily quantified and reproduced with the commercial MTT bioassay. (2) mPCLS were successfully adhered with NuSil® silicone-based adhesive and withstood air blowing on a sticky elastic membrane. (3) NuSil® adhesive does not release toxic byproducts that decrease viability. (4) Adhered mPCLS were cyclically stretched for 24 hours at average body temperature (37°C) to model *in vivo* mechanical ventilation and maintained viability.

Future studies building off this work will include creating a FlexFrame blueprint to position PCLS on the center of the membrane with equidistant application of NuSil® adhesive to ensure equibaxial stretch. Given the establishment of tissue viability, pharmacological antagonists or agonists can be tested on mPCLS. Cellular mechanics, inflammatory cytokine signal scope, and airway contractility experiments can be pursued

in murine and human PCLS with different genetic profiles and disease conditions.

Beyond investigation of the lung, this optimized bioassay system can be adopted to study other organs, like the bladder or uterus, which are subject to biomechanical forces.

BIBLIOGRAPHY

1. *Acute Respiratory Distress Syndrome (ARDS) Market to Reach a CAGR of 10.1% during 2024-2034, Impelled by Aging Population.* (2024, August 2). BioSpace. <https://www.biospace.com/acute-respiratory-distress-syndrome-ards-market-to-reach-a-cagr-of-10-1-during-2024-2034-impelled-by-aging-population>
2. Arnal, J.-M., Saoli, M., & Garnero, A. (2020). Airway and transpulmonary driving pressures and mechanical powers selected by INTELLiVENT-ASV in passive, mechanically ventilated ICU patients. *Heart & Lung: The Journal of Cardiopulmonary and Acute Care*, 49(4), 427–434. <https://doi.org/10.1016/j.hrtlng.2019.11.001>
3. Association, A. L. (n.d.). *What to Know if Your Loved One is Diagnosed with ARDS.* Retrieved November 21, 2024, from <https://www.lung.org/blog/ards-diagnosis-doctor-advice>
4. Bryda, E. C. (2013). The Mighty Mouse: The Impact of Rodents on Advances in Biomedical Research. *Missouri Medicine The Journal of the Missouri State Medical Association - Since 1904*, 110(3), 207–211.
5. Cave, C., Samano, D., Sharma, A. M., Dickinson, J., Salomon, J., & Mahapatra, S. (2024). Acute respiratory distress syndrome: A review of ARDS across the life course. *Journal of Investigative Medicine*, 72(8), 798–818. <https://doi.org/10.1177/10815589241270612>
6. *Critical Care—Acute Respiratory Distress Syndrome—Fast Facts | New England Journal of Medicine Resident 360.* (n.d.). Mms.Org. Retrieved November 26, 2024, from <https://resident360.nejm.org/rotation-prep/critical-care/ards/fast-facts>
7. Fan, E., Brodie, D., & Slutsky, A. S. (2018). Acute Respiratory Distress Syndrome: Advances in Diagnosis and Treatment. *Journal of the American Medical Association*, 319(7), 698–710. <https://doi.org/10.1001/jama.2017.21907>
8. Haddad, M., & Sharma, S. (2024). Physiology, Lung. In *StatPearls*. StatPearls Publishing. <http://www.ncbi.nlm.nih.gov/books/NBK545177/>
9. Hallett, S., Toro, F., & Ashurst, J. V. (2025). Physiology, Tidal Volume. In *StatPearls*. StatPearls Publishing. <http://www.ncbi.nlm.nih.gov/books/NBK482502/>
10. Han, S., & Mallampalli, R. K. (2015). The acute respiratory distress syndrome: From mechanism to translation. *Journal of Immunology (Baltimore, Md. : 1950)*, 194(3), 855–860. <https://doi.org/10.4049/jimmunol.1402513>

11. Hendrickson, K. W., Peltan, I. D., & Brown, S. M. (2021). The Epidemiology of Acute Respiratory Distress Syndrome Before and After Coronavirus Disease 2019. *Critical Care Clinics*, 37(4), 703–716. <https://doi.org/10.1016/j.ccc.2021.05.001>
12. Irvin, C. G., & Bates, J. H. (2003). Measuring the lung function in the mouse: The challenge of size. *Respiratory Research*, 4(1), 1. <https://doi.org/10.1186/rr199>
13. Khalef, L., Lydia, R., Filicia, K., & Moussa, B. (2024). Cell viability and cytotoxicity assays: Biochemical elements and cellular compartments. *Cell Biochemistry and Function*, 42(3), e4007. <https://doi.org/10.1002/cbf.4007>
14. Kim, J. H., Schaible, N., Hall, J. K., Bartolák-Suki, E., Deng, Y., Herrmann, J., Sonnenberg, A., Behrsing, H. P., Lutchen, K. R., Krishnan, R., & Suki, B. (2023). Multiscale stiffness of human emphysematous precision cut lung slices. *Science Advances*, 9(20), eadf2535. <https://doi.org/10.1126/sciadv.adf2535>
15. Koziol-White, C., Gebiski, E., Cao, G., & Panettieri, R. A. (2024). Precision cut lung slices: An integrated ex vivo model for studying lung physiology, pharmacology, disease pathogenesis and drug discovery. *Respiratory Research*, 25(1), 231. <https://doi.org/10.1186/s12931-024-02855-6>
16. Lam, M., Lamanna, E., Organ, L., Donovan, C., & Bourke, J. E. (2023). Perspectives on precision cut lung slices—Powerful tools for investigation of mechanisms and therapeutic targets in lung diseases. *Frontiers in Pharmacology*, 14, 1162889. <https://doi.org/10.3389/fphar.2023.1162889>
17. Landry, J. (2025). *Negative vs. Positive Pressure Ventilation (2025)*. Retrieved February 8, 2025, from <https://www.respiratorytherapyzone.com/negative-vs-positive-pressure-ventilation/>
18. Lehmann, M., Krishnan, R., Sucre, J., Kulkarni, H. S., Pineda, R. H., Anderson, C., Banovich, N. E., Behrsing, H. P., Dean, C. H., Haak, A., Gosens, R., Kaminski, N., Zagorska, A., Koziol-White, C., Metcalf, J. P., Kim, Y. H., Loebel, C., Neptune, E., Noel, A., ... Königshoff, M. (2025). Precision-Cut Lung Slices: Emerging Tools for Preclinical and Translational Lung Research: An Official American Thoracic Society Workshop Report. *American Journal of Respiratory Cell and Molecular Biology*, 72(1), 16–31. <https://doi.org/10.1165/rcmb.2024-0479ST>
19. Liao, X., Zhang, W., Dai, H., Jing, R., Ye, M., Ge, W., Pei, S., & Pan, L. (2021). Neutrophil-Derived IL-17 Promotes Ventilator-Induced Lung Injury via p38

- MAPK/MCP-1 Pathway Activation. *Frontiers in Immunology*, 12. <https://doi.org/10.3389/fimmu.2021.768813>
20. Liu, G., Betts, C., Cunoosamy, D. M., Åberg, P. M., Hornberg, J. J., Sivars, K. B., & Cohen, T. S. (2019). Use of precision cut lung slices as a translational model for the study of lung biology. *Respiratory Research*, 20(1), 162. <https://doi.org/10.1186/s12931-019-1131-x>
 21. Miles, L. (n.d.). *LibGuides: BIO 140 - Human Biology I - Textbook: Chapter 29 - Organs and Structures of the Respiratory System*. Retrieved November 19, 2024, from <https://guides.hostos.cuny.edu/bio140/7-29>
 22. Mondoñedo, J. R., Bartolák-Suki, E., Bou Jawde, S., Nelson, K., Cao, K., Sonnenberg, A., Obrochta, W. P., Imsirovic, J., Ram-Mohan, S., Krishnan, R., & Suki, B. (2020). A High-Throughput System for Cyclic Stretching of Precision-Cut Lung Slices During Acute Cigarette Smoke Extract Exposure. *Frontiers in Physiology*, 11, 566. <https://doi.org/10.3389/fphys.2020.00566>
 23. Pereira, N. L., Schaible, N., Desai, A., Chan, E. C., Ablooglu, A. J., Capuano, J., Lin, E., An, Z., Gebski, E., Jester, W., Ganesan, S., Balenga, N., Koziol-White, C., Panettieri, R. A., Choudhury, S., Krishnan, R., & Druey, K. M. (2024). N-cadherin antagonism is bronchoprotective in severe asthma models. *Science Advances*, 10(48), eadp8872. <https://doi.org/10.1126/sciadv.adp8872>
 24. Powers, K. A., & Dhamoon, A. S. (2024). Physiology, Pulmonary Ventilation and Perfusion. In *StatPearls*. StatPearls Publishing. <http://www.ncbi.nlm.nih.gov/books/NBK539907/>
 25. Quiros, K. a. M., Nelson, T. M., Sattari, S., Mariano, C. A., Ulu, A., Dominguez, E. C., Nordgren, T. M., & Eskandari, M. (2022). Mouse lung mechanical properties under varying inflation volumes and cycling frequencies. *Scientific Reports*, 12(1), 7094. <https://doi.org/10.1038/s41598-022-10417-3>
 26. Ram-Mohan, S., Bai, Y., Schaible, N., Ehrlicher, A. J., Cook, D. P., Suki, B., Stoltz, D. A., Solway, J., Ai, X., & Krishnan, R. (2020). Tissue traction microscopy to quantify muscle contraction within precision-cut lung slices. *American Journal of Physiology - Lung Cellular and Molecular Physiology*, 318(2), L323–L330. <https://doi.org/10.1152/ajplung.00297.2019>
 27. Research, C. for D. E. and. (2023). FDA authorizes Gohibic (vilobelimab) injection for the treatment of COVID-19. *FDA*. <https://www.fda.gov/drugs/drug-safety-and-availability/fda-authorizes-gohibic-vilobelimab-injection-treatment-covid-19>

28. Rosner, S. R., Ram-Mohan, S., Paez-Cortez, J. R., Lavoie, T. L., Dowell, M. L., Yuan, L., Ai, X., Fine, A., Aird, W. C., Solway, J., Fredberg, J. J., & Krishnan, R. (2014). Airway Contractility in the Precision-Cut Lung Slice after Cryopreservation. *American Journal of Respiratory Cell and Molecular Biology*, *50*(5), 876. <https://doi.org/10.1165/rcmb.2013-0166MA>
29. Seadler, B. D., Toro, F., & Sharma, S. (2024). Physiology, Alveolar Tension. In *StatPearls*. StatPearls Publishing. <http://www.ncbi.nlm.nih.gov/books/NBK539825/>
30. Silva, P. L., Scharffenberg, M., & Rocco, P. R. M. (2023). Understanding the mechanisms of ventilator-induced lung injury using animal models. *Intensive Care Medicine Experimental*, *11*, 82. <https://doi.org/10.1186/s40635-023-00569-5>
31. Slutsky, A. S., & Ranieri, V. M. (2013). Ventilator-Induced Lung Injury. *New England Journal of Medicine*, *369*(22), 2126–2136. <https://doi.org/10.1056/NEJMra1208707>
32. Swenson, K. E., & Swenson, E. R. (2021). Pathophysiology of Acute Respiratory Distress Syndrome and COVID-19 Lung Injury. *Critical Care Clinics*, *37*(4), 749–776. <https://doi.org/10.1016/j.ccc.2021.05.003>
33. The ARDS Definition Task Force*. (2012). Acute Respiratory Distress Syndrome: The Berlin Definition. *The Journal of the American Medical Association*, *307*(23), 2526–2533. <https://doi.org/10.1001/jama.2012.5669>
34. Viana, F., O’Kane, C. M., & Schroeder, G. N. (2022). Precision-cut lung slices: A powerful ex vivo model to investigate respiratory infectious diseases. *Molecular Microbiology*, *117*(3), 578–588. <https://doi.org/10.1111/mmi.14817>
35. von Düring, S., Parhar, K. K. S., Adhikari, N. K. J., Urner, M., Kim, S. J., Munshi, L., Liu, K., & Fan, E. (2025). Understanding ventilator-induced lung injury: The role of mechanical power. *Journal of Critical Care*, *85*, 154902. <https://doi.org/10.1016/j.jcrc.2024.154902>
36. Watson, C. Y., Damiani, F., Ram-Mohan, S., Rodrigues, S., de Moura Queiroz, P., Donaghey, T. C., Rosenblum Lichtenstein, J. H., Brain, J. D., Krishnan, R., & Molina, R. M. (2016). Screening for Chemical Toxicity Using Cryopreserved Precision Cut Lung Slices. *Toxicological Sciences*, *150*(1), 225–233. <https://doi.org/10.1093/toxsci/kfv320>
37. Yartsev, A. (n.d.). *Inspiratory pause, I:E ratio and inspiratory rise time / Deranged Physiology*. Retrieved January 5, 2025, from

<https://derangedphysiology.com/main/cicm-primary-exam/respiratory-system/Chapter-539/inspiratory-pause-ie-ratio-and-inspiratory-rise-time>

38. Yoshie, H., Koushki, N., Kaviani, R., Tabatabaei, M., Rajendran, K., Dang, Q., Husain, A., Yao, S., Li, C., Sullivan, J. K., Saint-Geniez, M., Krishnan, R., & Ehrlicher, A. J. (2018). Traction Force Screening Enabled by Compliant PDMS Elastomers. *Biophysical Journal*, *114*(9), 2194–2199. <https://doi.org/10.1016/j.bpj.2018.02.045>
39. Zaidi, S. F., Shaikh, A., Khan, D. A., Surani, S., & Ratnani, I. (2024). Driving pressure in mechanical ventilation: A review. *World Journal of Critical Care Medicine*, *13*(1), 88385. <https://doi.org/10.5492/wjccm.v13.i1.88385>

CURRICULUM VITAE

